Aus dem Fachbereich Medizin
der Johann Wolfgang Goethe-Universität
Frankfurt am Main

betreut am
Zentrum der Hygiene
Institut für Medizinische Virologie
Direktorin: Prof. Dr. Sandra Ciesek

Characterization of Antiviral Effects of Emricasan and SARS-CoV-2 Isolates in Vitro

Dissertation
zur Erlangung des Doktorgrades der Medizin
des Fachbereichs Medizin
der Johann Wolfgang Goethe-Universität
Frankfurt am Main

vorgelegt von
Annika Eby Pfeiffer

aus Heidelberg

Frankfurt am Main, 2023

Aus dem Fachbereich Medizin
der Johann Wolfgang Goethe-Universität
Frankfurt am Main

betreut am
Zentrum der Hygiene
Institut für Medizinische Virologie
Direktorin: Prof. Dr. Sandra Ciesek

Characterization of Antiviral Effects of Emricasan and SARS-CoV-2 Isolates in Vitro

Dissertation
zur Erlangung des Doktorgrades der Medizin
des Fachbereichs Medizin
der Johann Wolfgang Goethe-Universität
Frankfurt am Main

vorgelegt von
Annika Eby Pfeiffer

aus Heidelberg

Frankfurt am Main, 2023

Dekan:	Prof. Dr. Stefan Zeuzem
Referent/in:	Prof. Dr. Denisa Bojkova
Korreferent/in:	Dr. Claudia Reinheimer
Tag der mündlichen Prüfung:	07.11.2023

Zusammenfassung

Die Auswirkungen der Covid-19-Pandemie erforderten rasche Reaktionen angesichts neuer Herausforderungen. In diesem Zusammenhang wurde es unabdingbar, mehr über den Erreger SARS-CoV-2 zu erfahren. Daher wurden klinische Virusisolate mit Schwerpunkt auf Infektiosität, Replikationskinetik und Caspasenaktivität untersucht.

Zunächst wurden klinische Proben von Patienten in Zellkultur auf Infektiosität getestet. Zusammen mit viralem RNA-Vorkommen untersucht in der Polymerase-Kettenreaktion, wurde aus diesen Ergebnissen eine Formel zur Vorhersage der Infektiosität in Zellkultur entwickelt. Zusätzlich wurde die Frage der Infektiosität durch die Analyse verschiedener Probentypen, Quellen und Materialien beleuchtet. Hier wurde Infektiosität von Proben aus verschiedenen Teilen des Respirationstrakts nachgewiesen, darunter auch Proben, die von Verstorbenen stammen. Es wurde ein Protokoll für die Virusisolierung auf menschlichem Atemwegsepithelzellen in Luft-Flüssigkeits-Interface-Kultur erstellt.

Zweitens wurde die Replikationskinetik von 20 klinischen Isolaten verglichen, einschließlich einer Untergruppe von sieben sequenzierten Isolaten. Alle Isolate konnten in dem Zellkulturmodell aus Kolonepithel replizieren. Innerhalb der Untergruppe wurden Unterschiede zwischen Isolaten beobachtet, die den D614G-Aminosäureaustausch tragen im Vergleich zu denen mit originalem Spike-Protein.

Schließlich wurde eine erhöhte Caspasenaktivität in zwei Zellkulturmodellen nachgewiesen, darunter menschliche Atemwegsepithelzellen in Luft-Flüssigkeits-Interface-Kultur. Anschließend wurde Caspaseninhibition durch die niedermolekulare Verbindung Emricasan und ihre Auswirkungen auf den in der Zellkultur beobachteten zytopathischen Effekt untersucht. Dabei wurde eine erhöhte Zellüberlebensrate in einer Kolonepithelzelllinie bei ungestörter Virusreplikation nachgewiesen. Erhöhte Caspasenaktivität wurde als früher Marker für eine Infektion identifiziert und durch Tests mit 20 klinischen Virusisolaten validiert.

Diese Studie liefert Informationen zur Infektiosität, die zum Verständnis des Übertragungsrisikos beitragen können. So wurden Teile der hier gesammelten Daten für die Validierung von Antigen-Schnelltests verwendet. Die durch die Untersuchung der Caspasenaktivität gewonnenen Erkenntnisse trugen zum Teil zur Entwicklung einer Arzneimittel-Screening-Methode durch Bojkova et al.[41] bei und können so Arbeitsroutinen im Labor erleichtern. Es konnte gezeigt werden, dass Emricasan keine antivirale Wirkung hat, während die Feststellung einer erhöhten Zellüberlebensrate in Zellkulturen Anlass zu weiterer Forschung zur Prävention von Gewebeschäden geben könnte.

Summary

The impact of the Covid-19 pandemic called for rapid responses in face of unprecedented challenges. In this context, earning more about the causative agent SARS-CoV-2 becomes imperative. Therefore, clinical virus isolates were studied with focus on infectivity, replication kinetic, and caspase activity.

Firstly, clinical specimens collected from patients were tested for infectivity in cell culture. Combined with polymerase chain reaction results, a formula predicting infectivity in cell culture based on abundance of viral RNA was developed. Additionally, analysis of different specimen types, sources, and material, elucidate the question of infectivity. Here, infectivity was demonstrated in specimens derived from different parts of the respiratory tract, including specimens collected from deceased persons. A protocol for virus isolation on human airway epithelium in air-liquid interface culture was established.

Secondly, replication kinetics of 20 clinical isolates were compared, including a subset of seven sequenced isolates. All isolates replicated in the colon epithelial cell culture model. Within the subset, differences between isolates carrying the D614G amino acid exchange and with original spike protein were observed.

Lastly, elevated caspase activity was demonstrated in two cell culture models including human airway epithelium in air-liquid interface culture. Subsequently, caspase inhibition by small-molecule compound Emricasan and its effects on the cytopathic effect observed in cell culture were studied. Here, increased cell survival in a colon epithelial cell line was shown with unimpaired virus replication. Elevated caspase activity was identified as early marker of infection and validated by testing across 20 clinical virus isolates.

This study offers information on infectivity that can help shape the understanding of transmission risk. As such, parts of the data collected here were used for validation of rapid antigen tests. The insights gained by studying caspase activity contributed in part to the development of a drug screening method by Bojkova et al.,[41] thus aiding routine laboratory workflow. It was demonstrated that Emricasan exhibits no antiviral effect, while the finding of increased cell survival in cell culture could give rise to further research on prevention of tissue damage.

Table of Contents

1 Introduction

The Covid-19 pandemic has challenged society in an unprecedented way, Johns Hopkins University reporting close to 6.9 million deaths up to March, 2023.[1] The causative agent, a betacoronavirus now named SARS-CoV-2, was identified in December 2019 in association with a pneumonia outbreak.[2]

1.1 Virologic research in public health policies

“Flatten the curve”, i.e., reducing exponential spread to a rate manageable for health care systems, became a popular visualization of public health containment measures.[3,4] This underlines the importance of understanding infectivity when implementing isolation and quarantine measures, as seen in World Health Organization and Robert Koch-Institute recommendations.[5,6] Although polymerase chain reaction (PCR) is readily available to detect viral RNA and identify infected persons, it is not possible to directly infer infectivity based on presence of viral RNA alone. Instead, epidemiologic and virologic research is needed, with virus isolation in cell culture as surrogate marker for infectivity. From a virologic perspective, the ability of infecting cells in vitro provides evidence of viable virus in a given specimen, i.e., a nose swab. In a second step, the infectivity of the specimen source can be inferred. Hence, this model simplification can help identify the infectious period.[7-9] In combination with epidemiologic data, it is also possible to gain insight into the temporal profile of the disease, i.e., the incubation period.[10,11] However, there are two main obstacles impeding research on virus isolation: Firstly, SARS-CoV-2 isolation in cell culture to this day requires BSL-3 working conditions. Secondly, a cell culture system that is robustly susceptible to infection must be established. These factual limitations highlight the responsibility of adequately equipped institutions to study infectivity.

1.2 Taxonomy and replication cycle

Coronaviruses are enveloped positive-sense single strand RNA viruses that use spike proteins to specifically bind to the host cell receptor.[12] While human coronaviruses such as HCoV-229E, an Alphacoronavirus, or HCoV-OC43, a more closely related betacoronavirus from a different subgenus, are endemic and usually cause “common colds”, newly emerging pathogens are prone to causing severe disease, as was the case with SARS and MERS.[12,13] Upon entry, SARS-CoV-2 spike protein binds to ACE2 with the receptor binding domain (RBD), protease-dependent cleavage mediated mainly by transmembrane protease serine subtype 2 (TMPRSS2) or less frequently, when entering via the endosome, cathepsin L exposes the S2 subunit promoting membrane fusion and release of the positive-sense RNA for primary translation of two different polyproteins which harbor up to 16 non-structural proteins (nsp) depending on open reading frame (ORF).[14,15] After processing, these form the replication transcription complex (RTC) synthesizing new genomic RNA and a subset of subgenomic RNA for structural and accessory proteins.[12] The double-stranded RNA intermediate that originates from this process and can trigger an innate immune response is hidden inside a double-membrane vesicle as an example for immune evasion.[16] N-protein coated new genomic RNA buds into ER-to-Golgi-intermediate compartment containing structural proteins, thus acquiring a bilipid envelope.[12,14] After assembly is completed, the virion is released by exocytosis via the Golgi apparatus.[12]

Despite nsp14-exonuclease activity as proofreading mechanism, the high mutation rate typical of RNA-viruses amplified by the pandemic spread continues leading to variants.[17,18] Of particular interest are WHO-identified variants of concern with higher transmissibility, virulence or immune evasion.[19] Thus, the now prevalent D614G exchange was under scrutiny when it emerged in 2020, as it stabilizes a spike-protein conformation favorable to infection.[20,21] In this context, characterization of clinical specimens becomes important, as they may reflect phenotypes of currently circulating virus variants more accurately than laboratory

strains. Additionally, alterations to different steps of the replication cycle can be introduced through passaging in cell culture, producing cell culture artefacts that can introduce biases to in vitro research results in cell culture systems, as observed for instance with SARS-CoV-2 cultured in Vero E6-cells that lead to deletions in a protease cleavage motif at the spike-protein junction, attenuating the disease caused in animal models and altering entry.[22-24]

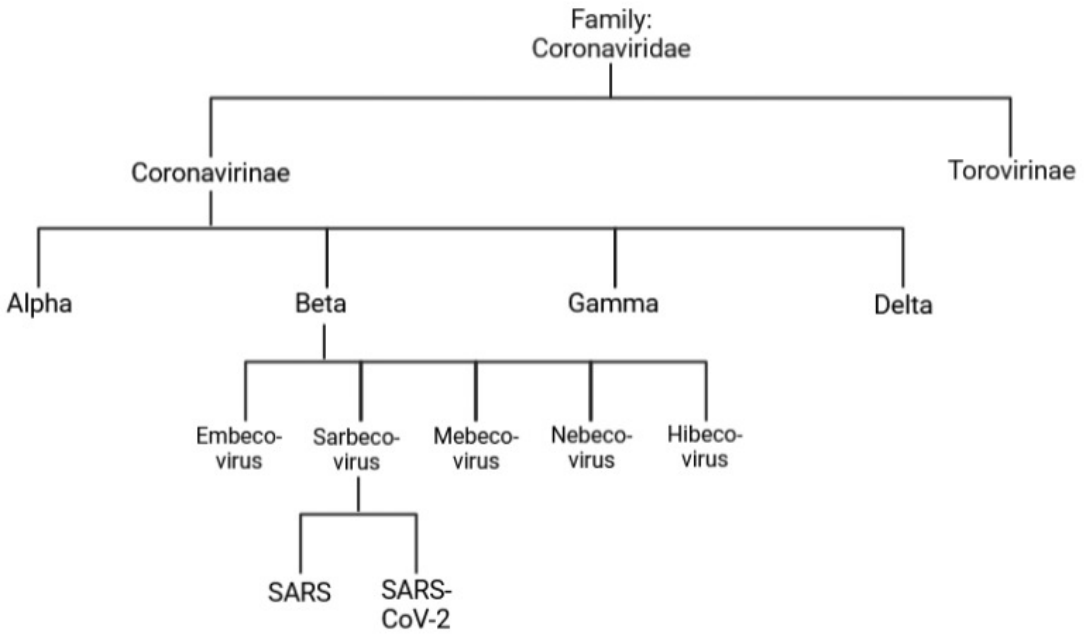

Illustration 1: Taxonomy. Modified from[13].

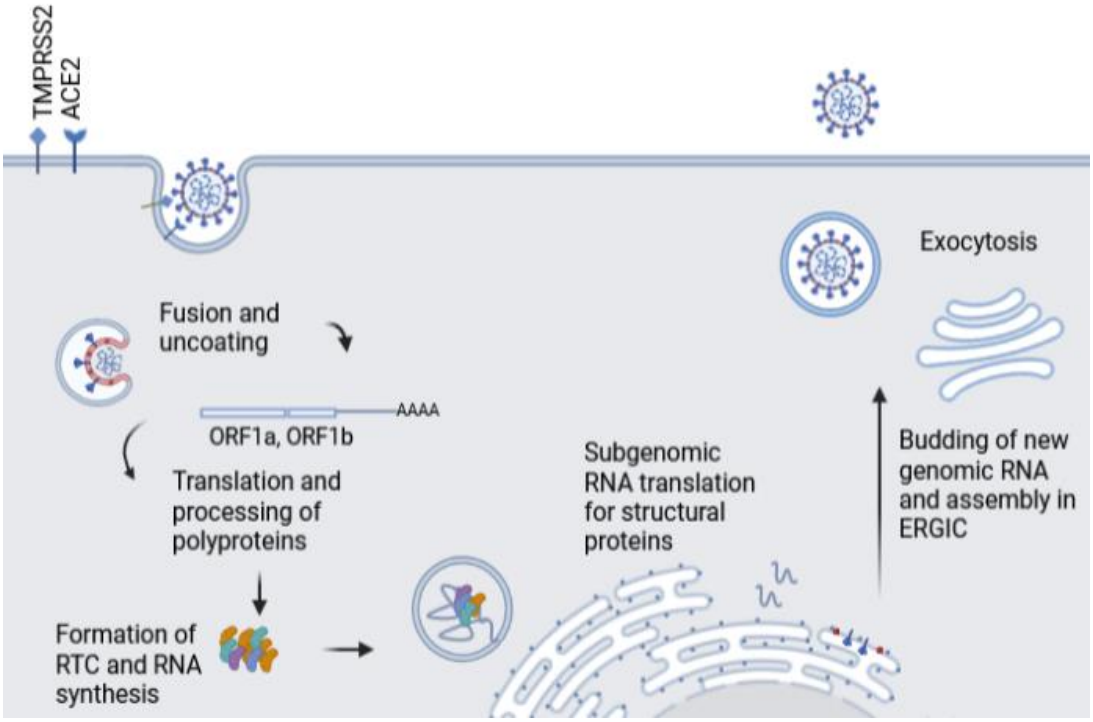

Illustration 2: SARS-CoV-2 replication cycle. Spike protein binds to ACE2, TMPRSS2 or cathepsin-mediated cleavage promotes fusion. After release of the genomic RNA, translation leads to two distinct polyproteins depending on whether ribosomal frameshift enables ORF1b translation. Polyprotein processing results in 16 nonstructural proteins that form the replication transcription complex and synthesize new genomic RNA and subgenomic RNA encoding structural and accessory proteins. Genomic RNA budding into the ER-to-Golgi-intermediate compartment initiates assembly. New virions are released by exocytosis. Modified from[12] and[14].

1.3 Covid-19 disease

Covid-19 is a primarily respiratory infectious disease with extrapulmonary complications. From today's perspective in 2023, the prominent patient-inherent risk factor is advanced age: Hospitalization rate for the 65 to 74-year age group is five times higher and death 60 times more frequent than in the ages 18 to 29-year old reference group in the American demographic, both rates increasing in older comparison groups.[25] Overall, about 15% of cases develop severe and 5% critical disease.[26] Omicron, the prevalent variant in 2023, is associated with more gastrointestinal symptoms and generally lesser severity, possibly due to predominant replication in the upper respiratory tract instead of the lungs, however epidemiological data on virulence must be interpreted in the context of an increasingly immune population.[27,28] This study was conducted in 2020 when Covid-19 was a newly emerging disease and the D614G amino acid exchange became prevalent.[29]

Mild Covid-19 clinically presents with cold-like symptoms, i.e. cough, fever, fatigue, rhinitis, pharyngitis, occasionally anosmia, dysgeusia, and gastrointestinal symptoms.[30,31] While asymptomatic infections are described, severe Covid-19 manifests usually within the second week as interstitial pneumonia with hypoxaemia, potentially leading to acute respiratory distress syndrome (ARDS), multiple organ failure, and septic shock as characterized in

the WHO Clinical Progression Scale.[32] Complications include endothelial dysfunction with hypercoagulability, as well as kidney, liver, central nervous system, and myocardial injury.[33,34] In children, a rare complication is pediatric inflammatory multisystem syndrome (PIMS).[35] A poorly understood late complication is Long-Covid or post-Covid 19 syndrome, a syndrome similar to and with some overlap to myalgic encephalomyelitis or chronic fatigue syndrome (ME/CFS).[26,34] There are four phases proposed to characterize the non-linear disease progression, namely ‘early viral upper respiratory non-hypoxic phase’ with mild symptoms, ‘early inflammatory lower respiratory hypoxic phase’ where pulmonary support may become necessary, the ‘second symptomatic phase’ with immune-related phenomena, and the ‘late phase’ at which point chronic manifestations may occur.[34,36]

Pathomechanistically, tissue damage and disease are attributed to virus replication and dysregulated immune response.[37,30] As a first defense barrier, innate immunity recognizes patterns typical of RNA-viral infection both intra- and extracellularly resulting in specialized immune cell activation, e.g. alveolar macrophages, as well as interferon and nuclear factor-κB induced chemokine and cytokine signalling.[38] However, SARS-CoV-2 attenuates this first antiviral response from different angles. Interferons I and III levels, alveolar macrophages, dendritic, and natural killer cells are decreased following infection, especially in severe cases, while proinflammatory cytokines and chemokines increase.[39,38,33] Concerning adaptive immune response, neutralizing antibodies mainly target epitopes within the RBD prone to change in emerging new variants and T-cell lymphopenia due to sequestration and apoptosis driven by proinflammatory cytokines in severe cases impedes this response as well.[38,40] The immunosuppressant aspect of infection combined with partial overactivity characterizes the dysregulated immune response.[38,33,41] On the macroanatomic and radiologic level, lung autopsies of severe cases show bilateral infiltrates or ground glass opacities.[42,43] This translates histopathologically to exudative diffuse alveolar damage with infiltrating immune cells, capillary congestion up to thromboembolism, syncytia formation, hyaline membranes, fibrosis and activated type II pneumocytes.[43-45] In general, as autopsied bodies show little signs of

replicating virus contrasting with high levels of immune cells and the alveolar cells show low levels of viral RNA despite high extent of destruction, a strong immunological component to tissue damage seems plausible.[38,46,47] Nonetheless, tissue damage also occurs directly through virus replication, e.g. in epi- and endothelial cells, and inability to prevent replication in early phases of the disease is considered as predisposition towards dysregulated proinflammatory disease and tissue damage.[38,30] For example, one study showed SARS-CoV-2 stimulates profibrotic monocytes directly in vitro, presumably worsening lung fibrosis in vivo.[48] The idea of a balanced immune response to help fight the disease consisting of replication containment and reduction of excess inflammation is reflected in pharmaceutical therapeutic approaches.

Antiviral substances are recommended during early phases of disease for persons at risk of developing severe disease, as this is when virus replication is highest rendering treatment most effective.[34] Due to interactions with the cytochrome P450 family and side effects outweighing the benefits, later administration is not advised.[49] Molnupiravir, Remdesivir, and Nirmatrelvir/Ritonavir are highlighted in German treatment guidelines.[49] Monoclonal anti-spike antibodies, e.g. Sotrovimab, are other candidates for early phase risk populations, in part with reduced neutralizing properties due to virusevolution.[50,49,51] However, the preventative nature of this treatment option, combined with intravenous administration for Remdesivir and Sotrovimab complicate efficient treatment in practice, especially in outpatient settings.[49] Secondly, immunomodulatory pharmaceutical interventions comprise glucocorticoids, namely dexamethasone supported with the strongest evidence for severe cases.[49,52] To a lesser degree of certainty, IL-6-receptor-antagonist Tocilizumab or JAK-inhibitor Baricitinib are also recommended for severely diseased patients.[49] As severe disease usually manifests in later stages of disease, the immunomodulatory drugs present a therapeutic option for when antiviral approaches are no longer sensible.[34] Thirdly, patients with risk factors benefit from prophylactic anticoagulatory pharmacotherapy, highlighting the importance of thromboembolic events as pathomechanism.[16] Treatment of post-

Covid 19 syndromes, as well as improvement of treatment options of acute disease, remain subject to research.

1.4 Caspase 3/7 activity

Caspases are traditionally regarded as key operators in apoptosis, a programmed cell death.[53] More specifically, caspase 3 and caspase 7 as executioner or effector caspases downstream of both extrinsic and intrinsic pathways are frequently described as cellular markers of apoptosis.[54,55] A highly regulated process, apoptosis comprises cell shrinkage with chromatin condensation forming pyknosis, blebbing, and fragmentation.[56-58] Characteristically, cellular debris is enveloped in parts of the cellular membrane and the dying cell is quickly removed causing little to no inflammation.[56,59,60] As new cell death pathways are identified, the former clear distinction of programmed without versus unprogrammed cell death with subsequent inflammation is blurred. Accordingly, caspase involvement has been demonstrated in pro-inflammatory pathways.[61,62] In virus infections, caspases can also take on ambivalent roles. On the one hand, apoptosis is an effective way to mitigate loss, i.e., let cell death occur before infection can spread beyond the infected cell.[63] Similarly, caspase involvement in pro-inflammatory pathways with ensuing immune response are detrimental to virus replication. Unsurprisingly, some viral proteins can inhibit caspases, possibly resulting in increased viral spread.[54] Conversely, apoptotic bodies can be used as virion-vehicles facilitating viral spread, as seen in influenza virus infection, and caspase activity can also be harnessed to activate viral proteins.[64-66] In MERS and SARS-CoV-2 infection, caspase 9 inhibition reduced lung hemorrhage and inflammatory cell infiltration in a transgenic human ACE2 mouse model, while also reducing inflammatory markers IL-6, IP10, and TNFα.[67] Caspase-mediated processes, i.e. elevated levels of apoptosis or caspase 1-associated inflammasome, are also present in Covid-19, alluding to pathogenetic relevance.[67,40,42,68]

1.5 Pan-caspase inhibitor Emricasan

Regardless of the effect on viral infection, while apoptosis also occurs physiologically, increased caspase activity has been observed in various diseases with tissue damage.[69] In ARDS for instance, apoptosis of pneumocytes types I and II leads to alveolar epithelial injury.[70] Presumably, injured lung tissue is then repaired inefficiently, a possible explanation for hyperplasia of less differentiated type II pneumocytes, reducing regeneration capacities and resulting in an overall decrease of type I pneumocytes as seen in Covid-19 pneumonia and ARDS.[16,43] Rescue of alveolar cells could thus hypothetically alleviate progression of ARDS. In other contexts, caspase inhibition has been pharmacologically targeted. Orally administrable small-molecule pan-caspase inhibitor Emricasan was originally developed for treatment of liver cirrhosis with an increased rate of apoptosis.[71,72] In the past, clinical trials reported mixed results: favorable with reduction of liver fibrosis in patients with moderate fibrosis, and discouraging, i.e. termination in phase II due to high systemic values as basis for concerns about hepatotoxicity, and no significant improvement without signs of toxicity in acute-on-chronic liver failure.[73,74-76] Contrary to valid concerns about oncogenic potential, this was not found in the animal model.[77] Moreover, it is also being discussed whether caspase inhibition could reduce apoptosis-induced proliferation as unwanted side effect of chemotherapy.[78] However, the clinical relevance of this phenomenon is yet to be determined. In Zika-infected neuronal progenitor cell culture models, this agent acted cytoprotectively, prompting the question on its faculties in Covid-19, as another RNA-virus-caused disease.[79] Via Caspase 1 inhibition upstream of pyroptotic cell death, it was proposed as treatment option after it was demonstrated that lymphocytes displayed heightened levels of Caspase 1 activity in Covid-19 patients.[80,81] However, the trial was terminated due to recruitment difficulties, no serious adverse events were reported.[81] Emricasan has also been identified as inhibitor of recombinant SARS-CoV-2 main protease (Mpro), justifying further research, especially with viable virus.

1.6 Aim of study

The aim of the study is to characterize patient derived clinical SARS-CoV-2 isolates focusing on infectivity, replication kinetic, and caspase 3/7 activity, as well as study potential antiviral and cytoprotective effects of Emricasan in vitro.

Initially, to gain information on infectivity, virus isolation was attempted from clinical specimens and isolation success in cell culture was documented. As a newly emerging pathogen, it was also unknown how robustly the established in-house cell culture system would be susceptible to infection from clinical specimens. Therefore, the idea was to attempt isolation in large quantities and from different sources, thereby validating the cell culture system. As PCR testing became a widely employed diagnostic tool, the aim was also to further elucidate the relationship between PCR cycle threshold (ct) and infectivity in cell culture. As side product following the same rationale, parts of this study were also used for validation of rapid antigen-tests as published by Toptan et al., and Kohmer et al.[82,83]

Secondly, with new variants emerging, clinical isolates are observed for differences in replication kinetics. In general, a workflow allowing for research on clinical isolates including isolation, propagation, and subsequent experiments should be established.

Thirdly, the effect of infection on caspase 3/7 activity is studied. Moreover, after finding elevated activity levels, the effect of caspase inhibition in cell culture by pan-caspase inhibitor Emricasan was examined with focus on cytopathic effect formation and virus replication. Another aim is to establish increased caspase 3/7 activity as early maker of infection and find out whether this can be uniformly observed across a subset of different clinical SARS-CoV-2 isolates.

2 Materials and Methods

2.1 Materials

2.1.1 Chemicals and reagents

Table 1: Antibodies, chemicals, and reagents

Chemical and reagent	Supplier
Acetic acid	Carl Roth
Acetone	Carl Roth
Amphotericin B	Sigma-Aldrich
3-Amino-9-ethylcarbazole	Sigma-Aldrich
Antibody against mouse IgG, biotin conjugated	Dianova
Antibody against J2 double strand RNA	Abcam
Antibody against rabbit IgG, Alexa fluor	Invitrogen
Antibody against rabbit IgG, peroxidase conjugated	Jackson ImmunoResearch
Antibody against SARS-CoV-2 spike S1 protein	Sino Biological
BSA (bovine serum albumin)	Sigma-Aldrich
DAPI	Thermo Scientific
***N,N*-Dimethylformamide**	Carl Roth
EDTA-Sodium (Titriplex III)	Merck
Glutamine	Sigma-Aldrich
Hydrogen peroxide	Merck
Methanol	Sigma-Aldrich
Milli-Q water	Merck
FCS (fetal calf serum)	Sigma-Aldrich

Goat serum	Gibco
Penicillin/streptomycin, 10000 ug/mL	Merck
Polysorbate 20	Sigma-Aldrich
Primocin	Invivogen
Sodium acetate	Carl Roth
Sodium chloride	Carl Roth
SDS (sodium dodecyl sulphate)	Carl Roth
Streptavidin-peroxidase-conjugate	AppliChem
Thiazolyl blue (MTT, 3-(4,5-dimethylthiazol-2-yl)-2,5-diphenyltetrazolium bromide)	Carl Roth
Thimerosal	Sigma-Aldrich
Tris(hydroxymethyl)aminomethan	Sigma-Aldrich
Triton X-100	AppliChem
Trypsin	Sigma

2.1.2 Labware

Table 2: Labware

Labware	**Supplier**
175 cm^2 cell culture flask	Corning
12.5 cm^2 cell culture tube	Thermo Scientific
Transparent 96 well microtiter plate	Greiner Bio-One
White 96 well microtiter plate	Greiner Bio-One
Conical centrifuge tube	Corning
Cryotube	Thermo Scientific
Conical microcentrifuge tube	Eppendorf
Open silicone ultracentrifuge tube	Thermo Scientific

2.1.3 Kits

Table 3: Kits

Kit	Supplier
Caspase-Glo® 3/7 Assay System	Promega
Luna® Universal One-Step RT-qPCR Kit	New England Biolabs
QIAamp Viral RNA Mini kit	Qiagen
QIAamp Viral RNA Mini QIAcube Kit	Qiagen

2.1.4 Buffers and media

Table 4: Buffers

Buffer	Composition
PBS (phosphate buffered saline)	137 mM NaCl 2.7 mM KCl
Washing buffer	60.6 g Tris 500 mM 87.7 g NaCl 1.5 mM
Cell lysis and Caspase 3/7 activity reagent	10% Caspase-Glo 3/7 Assay Caspase activity reagent 90% Triton X, 1%
Glutamine solution	29.2 g L-Glutamine Ad 1 L Milli-Q water
Blocking solution	400 mL washing buffer pH 7.45 8 g BSA 20 mL goat serum, 0.01% (w/v) Thimerosal
AEC solution	0.18 g AEC 45 mL *N,N*-Dimethylformamide

	105 mL Acetatebuffer pH 5
Trypsin solution	2.0 g Trypsin 0.6 g Titriplex III Ad 1 L PBS 0.2 µm filtrated
MTT reagent	2 mg/mL (w/v) in PBS
SDS solution	20% (w/v) SDS 50% (v/v) N,N-Dimethylformamide Ad acetic acid to pH 4.7
Sucrose-solution	20% (w/v) Sucrose Ad 1 L Milli-Q water

Table 5: Media

Medium	**Composition**
Minimum essential medium Eagle (MEM; Sigma Aldrich)	Formulated by the manufacturer: + 100 IU/mL penicillin + 100 µg/mL streptomycin + 5% Glutamine solution for cell culturing: + 10% FCS for virus stock propagation: + 1% FCS for virus isolation: + 1% FCS + 7.5 µg/mL Amphotericin B + 0.1 mg/mL Primocin
PneumaCult™-ALI Basal Medium (Stemcell)	Formulated by the manufacturer

2.1.5 Instruments

Table 6: Instruments

Instrument	Supplier
Thermo cycler with Bio-Rad CFX Manager software, version 3.1	Bio-Rad Laboratories
Nucleic acid extractor	Qiagen
Microplate reader (immuno-cytochemistry)	Bio-Sys
Microplate reader (absorption and luminescence)	Tecan
Microplate reader (immuno-fluorescence)	Tecan
Centrifuge	Hettich
Ultracentrifuge	Beckman-Coulter

2.1.6 Cells

Table 7: cell lines

Cell line	Supplier
Human colon carcinoma (Caco-2 and Caco-2-F03)	Caco-2: DSMZ, Braunschweig, Germany, no.: ACC 169 Caco-2-F03: pre-selected for high viral infection permissiveness through passaging by Institute of Medical Virology, University Hospital Frankfurt am Main, Goethe University, 60590 Frankfurt am Main, Germany and

	available at Resistant Cancer Cell Line collection: (https://research.kent.ac.uk/industrial-biotechnology-centre/the-resistant-cancer-cell-line-rccl-collection/)
Human airway epithelium, nasal and bronchial	Kindly provided by Carla Bellinghausen and Marco Bechtel, University Hospital Frankfurt am Main, Goethe University

2.1.7 Virus strains

Table 8: Virus strains

Virus	**Supplier**
SARS Hong-Kong	Jindrich Cinatl, Institute for Medical Virology, University Hospital Frankfurt am Main, Goethe University
SARS-CoV-2 Isolates FFM1-7	Denisa Bojkova, Institute for Medical Virology, University Hospital Frankfurt am Main, Goethe University
SARS-CoV-2 Isolates FFM 8-20	Isolated as specified below

2.2 Methods

2.2.1 Clinical specimen preparation

Clinical specimens, except for specimens obtained postmortem in four cases and patient environment samples, were collected and analyzed by quantitative reverse transcriptase polymerase chain reaction (RT-qPCR) for diagnostic purposes. In all respiratory specimens included for further analysis, SARS-CoV-

2 RNA was detected by a clinical diagnostic laboratory prior to testing in cell culture.

As previously published,[82,84,83,85] clinical specimens, including sputum, swabs and tracheal secretions were stored at 4 °C. For the postmortem cohort, tissue samples and swabs were stored at -80°C until directly before preparation. Approximately 0.5 cm^3 thawed tissue specimen was dissected from original sample material and homogenized with 300 µL PBS. Tissue homogenates, swabs, sputum, and tracheal secretions were mixed with MEM containing volumetric 1% FCS, 3% Amphotericin B and 0.2% Primocin. Inocula derived from swab-, sputum, and tracheal secretion were directly transferred to Caco-2-F03 cells seeded in 5.5 cm^2 culture tubes, while tissue-inoculum was transferred to Caco-2-F03 cells after clearing by centrifugation and filtration with a 0.45 µm filter. Cytopathogenic effect (CPE) was assessed by light microscope for up to seven days. After a maximum of seven days or when CPE formation reached a plateau, supernatants were inspected for presence of SARS-CoV-2 viral RNA (vRNA) by RT-qPCR. Infected cell culture tubes including cells were stored at -80°C until further virus propagation.

For isolation on bronchial human airway epithelium (HAE) cultured on filters with basal medium and thus allowing an air liquid-interface (ALI), cells were washed three times with PBS to remove mucous secretions. Thereafter, cells were apically submerged in two times 500 µL inoculum for one hour, respectively.

2.2.2 Cell culture and virus stocks

Human colon carcinoma cell line (Caco-2) was previously inadvertently selected for high SARS-CoV and SARS-CoV-2 infection permissiveness through in-house passaging routines.[85] The emerging subline Caco-2-F03 displays higher ACE2, TMPRSS2 levels and CPE formation after SARS-CoV and SARS-CoV-2 infection[85]. Caco-2 cells were cultured in flasks or wells in MEM supplemented with 10% FCS, 4 mM L-glutamine, 100 IU/mL penicillin, and 100 g/mL streptomycin until confluency. Trypsin/EDTA was used for cell detaching. After

reaching confluency in 175 cm^2 flasks, cells were expanded at a ratio of 1:3. For 96 well microtiter plates, cells were seeded at 50000 per well. The cell line was regularly authenticated by short tandem repeat analysis and tested for mycoplasma contamination.

During virus propagation for stocks or virus experiments, medium was supplemented with 1% FCS instead of 10%. For virus stocks, RT-qPCR positive cell culture tubes that had previously displayed CPE were thawed and 1 mL supernatant including viral particles and cell debris was used for propagation in 175 cm^2 cell culture flasks containing Caco-2 cells at confluency. After two to three days, i.e., when cell lysis plateaued, cell culture flasks were frozen at -80°C. When thawed, supernatant was precleared by centrifugation at 2000 RPM for ten minutes at room temperature and stored in one mL aliquots. After virus quantification, confluent Caco-2 cells in 175 cm^2 cell culture flasks were infected at a multiplicity of infection (MOI) 0.1 and incubated until complete cell lysis. The resulting supernatant, again, was precleared after a freeze-thawing cycle and stored in aliquots at -80°C.

For ultracentrifuged virus stock, precleared virus stock was ultracentrifuged on a 20% sucrose cushion at 28000 rpm for two hours. The resulting pellet was resuspended in 300 µL PBS, aliquoted, and stored at -80°C.

ALI-HAE cultures were maintained with weekly changes of basal medium and apical washing with PBS. Previously, primary cells had been resuscitated, passaged once, seeded at $4*10^4$ and cultured on filters submerged in medium until confluency, as previously described.[105, 106] Subsequently, basal medium was replaced with maintenance medium, and apical medium was lifted off, allowing cells to differentiate.

2.2.3 RNA isolation and RT-qPCR

For RNA isolation, 100 µL cell culture supernatant was used following the manufacturer's instructions. SARS-CoV-2 RNA was analyzed by a SYBR Green-based, quantitative real-time reverse transcription polymerase chain reaction

(RT-qPCR) using primers targeting RNA-dependent RNA polymerase (RdRP) at 0.4 µM per reaction:

RdRP_SARSr-F2 (GTGARATGGTCATGTGTGGCGG)

RdRP_SARSr-R1 (CARATGTTAAASACACTATTAGCATA).

RNA copies were quantified using plasmid DNA standard curves (pEX-A128-RdRP) according to GenBank accession number NC_045512 RdRP target regions as previously described by Bojkova et al.[86] Thermal cycling conditions were set to 55 °C for ten minutes, 95 °C for one minute, a sequence of 95 °C for ten seconds followed by 60 °C for 30 seconds repeated 44 times, and a subsequent melt curve analysis step ranging from 60 to 95 °C. Software belonging to the thermocycler was used for analysis.

ORF1ab gene ct determined by the diagnostic department of the Institute for Medical Virology Frankfurt for diagnostic purposes were analyzed with cobas SARS-CoV-2 (Roche). Here, RNA copy numbers were calculated using a standard curve as published by Kohmer et al.[87]

2.2.4 Immunocytochemical staining

Cells were fixated with 100 µL acetone-methanol-solution per well in a 96 well microtiter plate format for ten minutes at room temperature. After incubation, the fixation solution was replaced with 25 µL blocking solution per well, i.e. donkey serum in PBS, to inhibit unspecific binding for a minimum of 30 minutes at 37°C for immediate continuation of the protocol or, alternatively, stored at 4°C until further processing.

Primary antibodies targeting SARS-CoV-2 S protein or double strand RNA were diluted to 1:1500 or 1:200 per µL washing buffer respectively, and incubated at 37°C for one hour, followed by two washing steps with 100 µL washing buffer per well in a 96-well format.

For S protein staining, after the primary anti-spike, biotin-conjugated antibody, a streptavidin-peroxidase conjugate at a dilution factor of 1:1000 per µL washing buffer was incubated for one hour at 37°C and excess removed with washing

buffer in two washing steps. Subsequently, AEC-solution, filtered and supplemented with 1% hydrogen peroxide, was applied and removed with washing buffer after ten minutes at 37°C.

For double strand RNA staining, a secondary anti-mouse, biotin-conjugated antibody was incubated at a dilution factor of 1:1000 per µL washing buffer for one hour at 37°C and removed by washing every well with 100 µL washing buffer three times. In a third step, a streptavidin-peroxidase-conjugate was incubated for one hour at 37°C at a dilution factor of 1:1000 per µL washing buffer. After three washing steps, AEC-hydrogen-peroxide solution was applied, incubated for ten minutes at 37°C and washed three times.

Immunocytochemical staining was observed visually under the light microscope and quantified using Bio-Sys plate reader and software. Results express the percentage of stained well surface.

2.2.5 Immunofluorescent labeling

Cells were fixated with 3% PFA and permeabilized with 0.1% Triton X-100. After a blocking step identical to immunocytochemical staining with donkey serum in PBS, spike antibody was added at a dilution of 1:1500. Subsequently, an immunofluorescent secondary antibody was added. Nuclei were stained with DAPI at a dilution of 1:1000. Fluorescent labeling was quantified automatically by a multiplate reader.

2.2.6 Virus quantification

Virus stock titers were assessed as 50% tissue culture infective dose ($TCID_{50}$). Cell culture supernatant containing viral particles was 100-fold diluted and transferred to 96-well microtiter plates cultured with confluent Caco-2 cells. For ultracentrifuged virus stock, initial dilution was 1000-fold. Ten-fold serial dilutions were performed in quadruplicates and incubated on cells with medium containing 1% FCS for three days. Thereafter, CPE was assessed visually under

a light microscope and documented. $TCID_{50}$ was calculated after Spearman-Kärber as described by Cinatl et al.[88,89]

2.2.7 Viral growth kinetics

Caco-2 cells were cultured in MEM, 10% FCS and seeded at 50000 per well in a 96 well microtiter plate format. When confluent, cells were inoculated with SARS-CoV-2 isolates at MOI 1 in 50 µL medium for one hour at 37°C. Subsequently, inoculum was removed and discarded, cells were washed twice with PBS and cultured in medium containing 1% FCS. Supernatant was harvested after ten, 24, and 48 hours post inoculation (hpi). RNA was isolated from 100 µL supernatant per well and analyzed by RT-qPCR. Cells were fixated and stained immunocytochemically targeting SARS-CoV-2 spike protein. Results are means from three independent experiments with triplicates for every isolate and were analyzed with GraphPad Prism software, version 8.

2.2.8 Caspase 3/7 activity

Caspase 3/7 activity reagent was diluted at a factor of 1:10 with Triton X-100, 1% directly before use. In parallel to growth kinetic experiments, confluent Caco-2 cells in 96 well microtiter plates were infected with SARS-CoV-2 isolates at a MOI 1, incubated at 37°C for one hour, followed by removal of inoculum, two PBS washing steps, and replaced with 100 µL medium, 1% FCS per well. At ten, 24-, and 48-hours post inoculation, 100 µL diluted Caspase activity reagent was added to each well, including three mock per microtiter plate. After 30 minutes at room temperature, 200 µL per well, i.e., the complete volume, was transferred to white microtiter plates for measuring.

For Caspase 3/7 activity measurement in human airway epithelium (HAE) in an air liquid-interface environment (ALI), cells were infected at a MOI 1 with ultracentrifuged virus suspended in PBS. Before infection, cells including mock were washed with 500 µL PBS per insert. The inoculum remained on cells for one

hour at 37°C and removed with three washing steps with PBS. Five days after inoculation, 100 µL PBS per insert was incubated on cells for 30 minutes at 37°C, harvested, and examined for viral RNA by RT-qPCR. One mL diluted Caspase reagent per insert including mock was incubated at room temperature for 1.5 hours, including 5 minutes plate shaking at 400-600 rpm, allowing complete cell lysis. Thereafter, the content of every insert was transferred to a white microtiter plate in portions of 200 µL for measuring.

Luminescence was recorded with a Tecan Infinite microplate reader. Results are means from three independent experiments in triplicates and were analyzed with GraphPad Prism software, version 8.0.

2.2.9 Compound dilution assay

Caco-2 cells were seeded at 5000 cells per well in a 96 well microtiter plate and cultured in medium containing 10% FCS until confluent. Medium was removed and replaced with serially diluted compound or mock suspended in 1% FCS medium. Medium containing viral particles was added immediately thereafter at a MOI 0.01. 24 and 48 hours after inoculation, supernatant was collected and inspected for viral RNA by RT-qPCR, Caspase 3/7 activity as per luminescence was measured, and cells were fixated and immunocytochemically marked for SARS-CoV-2 S protein. Results are means from three independent experiments using triplicates per condition and were analyzed using GraphPad Prism software, version 9.

Cytotoxicity was assessed by measuring MTT reduction in the absence of virus. Cells were treated with serially diluted compound or mock. After 24 and 48 hours, 25 µL MTT reagent was added to each well and let incubate for 4 hours, before adding 100 µL SDS reagent per well leading to cell lysis and crystals dissolving overnight at 37°C. Absorption was measured using a Tecan Infinite microplate reader at 620 and 690 nm. Results are presented as difference to vehicle-treated cells and were analyzed with GraphPad Prism software, version 8.0.

2.2.10 UV exposure

Medium containing viral particles was aliquoted into microcentrifuge tubes at equal volumes of 1 mL and exposed to UVC-radiation for ten minutes. Confluent Caco-2 cells in 96 well microtiter plates were then infected with UVC-exposed, non-exposed virus inoculum at a MOI 1, and mock-infected. After 24 hours, 5 µL supernatant per well were transferred to an empty microtiter plate and mixed with LDH assay storage buffer for storage at -80°C. Caspase 3/7 activity was measured in the remaining supernatant and cells, adding 95 µL instead of 100 µL reagent per well to maintain a 1:1 ratio and using undiluted reagent as supplied by the manufacturer. In parallel, cells were stained using primary antibodies targeting double strand RNA. Results are means from triplicates for every isolate and were analyzed with GraphPad Prism software, version 8.

2.2.11 Statistical analysis and visualization

Ct for SARS-CoV-2 ORF1 as determined by the diagnostic department of the Institute of Medical Virology, University Hospital Frankfurt am Main, were documented for all samples tested in cell culture. Predicted probability of successful virus isolation ($p(c)$) versus ct (c) was expressed as graph of a logistic regression curve using R. Based on the data collected, the function is of the form:

$$p(c) = \frac{1}{1 + e^{(-12.25184 + 0.42417 * c)}}$$

Multivariate logistic regression for specimen type analysis was performed using R version 4.1.2 (2021-11-01) and additional packages stats, ggplot2, aod, and readxl. Remaining graphs were plotted and analyzed using GraphPad Prism 8 software. Illustrations were created with BioRender.com. Unless stated otherwise, statistical significance between two groups was determined using two-tailed student's t-test and experiments repeated three times in triplicates. For three or more groups, ANOVA was used.

3 Results

3.1 Virus isolation

3.1.1 Low ct is linked to successful virus isolation

Diagnostically determined ct for clinical specimens that were evaluated in Caco-2 cell culture ranged from 14.96 to 38.53 (Figure 1 c.). In a first step, all 119 samples were tested for infectivity in cell culture (Figure 1 a., c.). This group included sampling materials derived from upper and lower respiratory tract (114), and non-respiratory tract organs (five). For the culture positive group, mean ct was 25.25 (standard deviation [SD]: 4.396; 1402850 copies/ mL; 95 % confidence interval [CI]: 24.09 - 26.41). Of these, in accordance with Koch's postulates, 20 isolates were propagated in cell culture, and after displaying CPE, aliquoted for future experiments. Within the culture negative group, mean ct was 31.82 (SD: 3.68; 13931 copies/ mL; 95 % CI: 30.88 - 32.76). Mean ct was significantly lower in the group displaying infectivity in cell culture ($p < 0.0001$). The highest ct observed in a cell culture positive specimen was 35.26, lowest ct rendering no virus isolation was 20.99. Of note, for two specimens with low ct, bronchoalveolar lavage and duodenal tissue collected during autopsy (ct 23.93 and 20.99, respectively), virus isolation failed. Mean ct in positive cell culture supernatants was 17.34 (95 % CI: 15.79 – 18.88) using 100 µL supernatant per sample. Assuming cell culture infectivity as proxy for potential transmissibility, it is possible to use these results to estimate infectivity. On the one hand, the broad range of sample type and origin affirms ct as reliable indicator, however outliers occurred, leaving room for further factors to explain infectivity. In total, as seen in the lower bound of the 95% confidence interval of this cohort, sample material with a ct ≥ 30.88 is likely not infectious. Reasons for infectivity despite high ct may be traced back to sample-inherent factors, such as virus and patient traits or external factors, such as technical issues, new PCR primers and protocols. In two cases that displayed ct > 30.88, samples were collected before April 2020 and from persons traveling internationally. Virus found in one of these two samples had been sequenced and identified as D614 variant.[90] Due to origin and early

timepoint in the course of the pandemic, lack of standardized PCR-protocols and possibly unknown virus traits may have contributed. This was not the case with the remaining three samples. It is possible that these samples were collected at the beginning of the infection, and therefore low amounts of viral RNA with a relatively high percentage of replicating virus are reflected in the high ct. Further follow-up data supporting this hypothesis, e.g., onset of symptoms, was not available.

Standard clinical sampling material is collected from the upper respiratory tract[91,8]. Analyzing viral loads found in this sample type may lead to clinically more accurate results when predicting infectiousness based on ct. Additionally, the presence of inhibitory and cytotoxic factors in tissue and blood may lead to false negative results in cell culture. Including specimens obtained only from the upper respiratory tract and excluding tissue, as well as multiple samples provided by the same individual, leaves a cohort of 109 in total, 56 cell culture positive (mean ct 25.37; 1289515 copies/mL; SD: 4.26; 95 % CI: 24.36 – 26.70), and 53 negative (mean ct 31.78; 14328 copies/ mL; SD: 3.45; 95 % CI: 30.95 - 32.84). At ct ≤ 24.91, all upper respiratory tract specimens were infectious in cell culture. Above 35.26, no cell culture positive specimens were observed.

For further analysis of infectivity in cell culture of specimens obtained from the entire respiratory tract in relation to ct, specimens were dichotomized according to their infectivity in cell culture (culture positive = 1, culture negative = 0). Using generalized linear models-function defined as binomial, a logistic regression analysis was performed with R. Calculated intercept and coefficient lead to the formula specified above (Materials and methods, 2.2.12). Consecutively, a curve expressing the predicted probability of positve cell culture versus ct was plotted (ct coefficient: -0.42, $p = 1.61*10^{-7}$, deviance: 95.409 on 107 degrees of freedom, AIC 99.409; Figure 1 b.). In summary, likelihood of virus isolation in cell culture increased with lower ct.

Fig.1

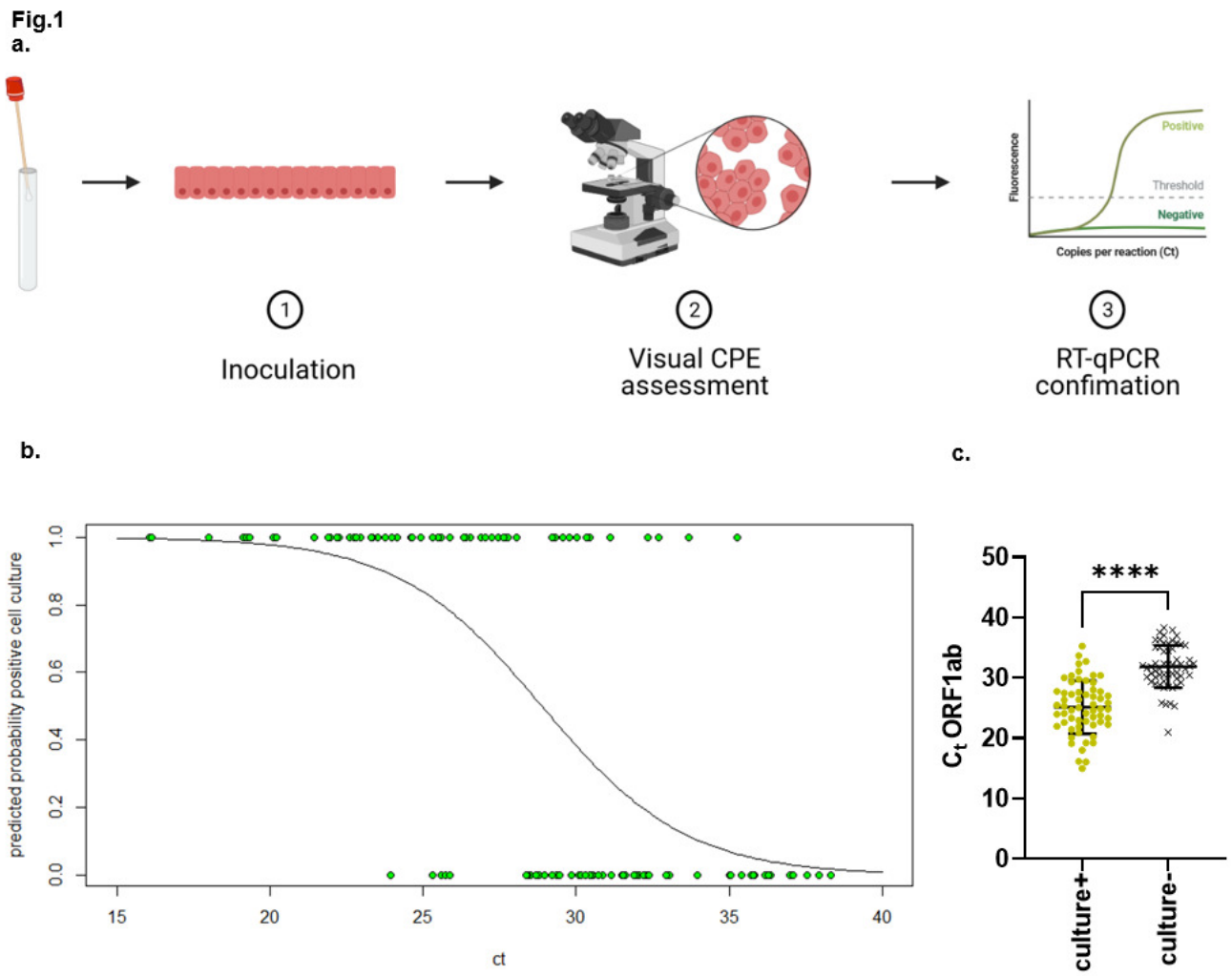

Figure 1: Low ct is linked to successful virus isolation.

a. *Establishment of workflow. Inoculum derived from clinical specimen is added to medium of Caco-2-F03 cells. CPE is assessed visually and confirmed by RT-qPCR.*
b. *Predicted probability of positive cell culture versus ct found in respiratory specimens, dichotomized as 1 = culture positive, 0 = culture negative.*
c. *Ct determined by diagnostic department containing non-respiratory and respiratory tract specimens.*

3.1.2 Virus isolation from different parts of the respiratory tract

Virus isolation was attempted from different sample materials from respiratory tract organs, non-respiratory tract organs, and patient environment (Figure 2 b. and d.). Viable virus was only isolated from specimens obtained from the respiratory tract. Oro-, nasopharyngeal, and not further specified respiratory swabs displayed similar ct (one-way ANOVA $p = 0.41$) with mean ct of 25.92, 29.43, and 29.07, respectively (Figure 2 a.). Accordingly, within cell culture positive and negative groups, mean ct did not differ significantly between these three groups (two-way ANOVA $p > 0.1$ for all groups). Analyzing positive cell culture versus ct and sample source site (naso-, oropharyngeal, respiratory not further specified, sputum, BAL) in a multivariate logistic regression model, only ct was significantly linked to positive cell culture ($p = 0.00048$ for ct, for samples types $p > 0.3$, ct coefficient; -0.35, deviance: 38.36 on 41 degrees of freedom, AIC: 50.36). Based on this data, no sample source site is particularly advantageous for successful virus isolation. Larger sample sizes are needed especially with respect to the sample types BAL and sputum. Additionally, the practice of combining naso- and oropharyngeal testing, a reportedly more sensitive testing option[92], could have hidden existing in vivo differences. However, while providing proof-of-concept evidence for potential infectivity of nasopharyngeal and oropharyngeal swabs and sputum, these findings do not allow exclusion of infectivity for other sample materials due to sample size.

To exclude interpersonal differences of infectivity and ct, sample materials from six persons that had given multiple samples were compared retrospectively (Figure 2 e.). The aim was to determine whether different sample material would lead to different results in viral culture. For four persons, samples were collected postmortem during autopsy, including tissue samples from non-respiratory organs. Swabs from the upper respiratory tract and sputum were collected from the remaining two persons. While viral RNA was detected in all persons, sample materials provided by only three proved culture positive. In two out of three subjects with positive cell culture samples, when viable virus was recovered from

one sample material, isolation also succeeded with the remaining samples. In this one exception, a cell culture negative oropharyngeal swab was collected postmortem from a subject with cell culture positive swabs from trachea, lungs and lung tissue.

In practice, this suggests that cell culture infectivity results can vary within one subject based on sample material origin. Conversely, collecting different samples materials can help achieve successful virus isolation. Due to small sample size, it is impossible to infer the frequency of this constellation.

To gather information on tenacity and alternative transmission routes, potentially contaminated surgical masks and filters used in ventilation devices were analyzed by RT-qPCR and in cell culture. RT-qPCR and cell culture testing of the used masks brought negative results (Figure 2 d.). As proof of concept, filters prepared with ultracentrifuged virus diluted with PBS to 10^4 and 10^7 $TCID_{50}$/mL were tested accordingly and yielded positive results after 24 and 48 hours (Figure 2 c.). Additionally, swabs collected from a patients' environment and auricle, rectum, armpit, and conjunctives remained culture negative (Figure 2 b.).

In total, while standardized testing is necessary for reliable data on tenacity, viable virus can under in vitro conditions be isolated after 48 hours. Here, masks, filters, and patient environment were found to be noncontagious. Further research updated to current variants under standardized conditions is warranted.

Fig. 2

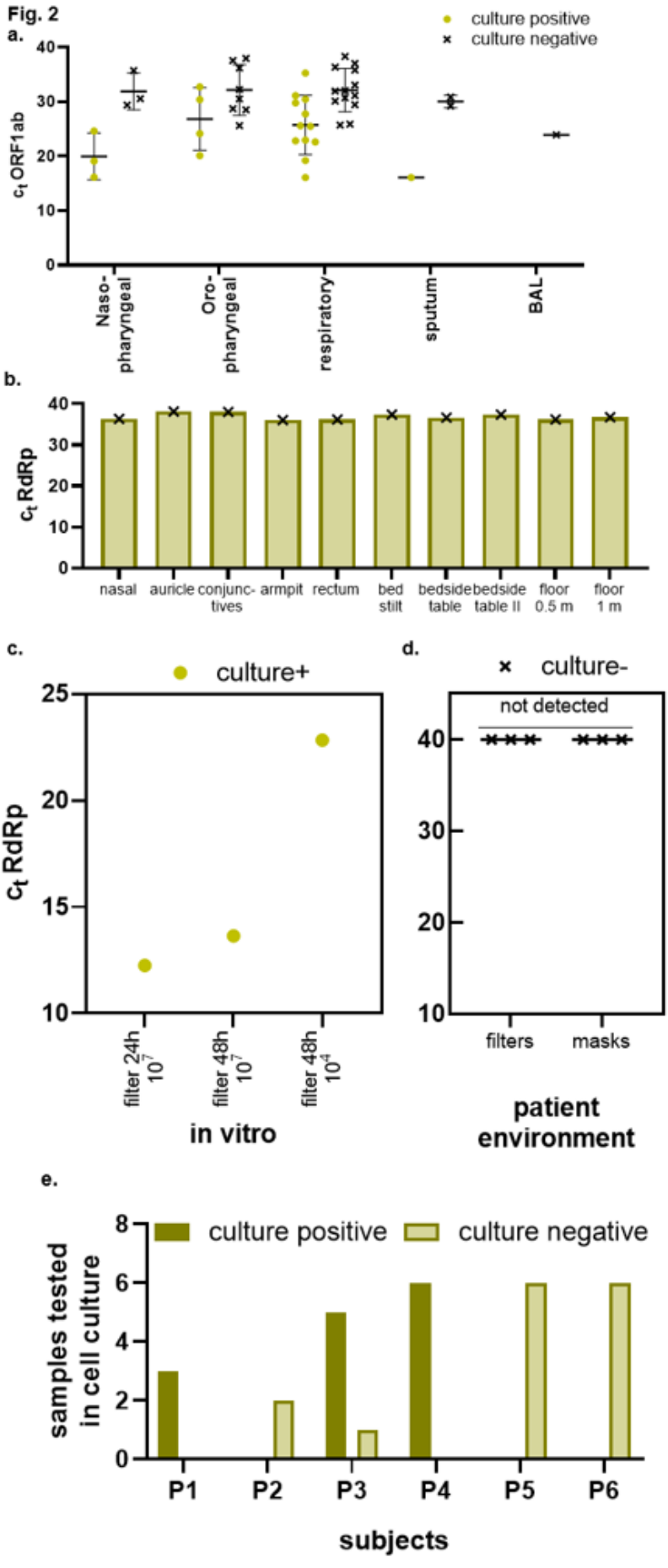
a.
culture positive
culture negative
c_t ORF1ab
Naso-pharyngeal
Oro-pharyngeal
respiratory
sputum
BAL
b.
c_t RdRp
nasal
auricle
conjunc-tives
armpit
rectum
bed stilt
bedside table
bedside table II
floor 0.5 m
floor 1 m
c.
culture+
c_t RdRp
filter 24h 10^7
filter 48h 10^7
filter 48h 10^4
in vitro
d.
culture-
not detected
filters
masks
patient environment
e.
culture positive
culture negative
samples tested in cell culture
P1
P2
P3
P4
P5
P6
subjects

Figure 2: Virus isolation from different parts of the respiratory tract.

a. *Respiratory clinical specimens sorted by sample source site. Comparison of sample source site reveal no significant difference.*
b. *Swab specimens collected from skin, conjunctives, rectum, and patient environment.*
c. *Virus isolation from prepared filters: inoculum derived from prepared filters was added to medium in cell culture, ct from supernatant and successful virus isolation (CPE + PCR) are shown. Filters were prepared at different TCID50/ mL and analyzed after 24 or 48 hours.*
d. *No virus isolation from used filters and masks.*
e. *Multiple specimens collected from six individuals. Number of specimens collected and result in cell culture are shown.*

3.1.3 Postmortem virus isolation

In order to assess viral load in organs and tenacity in bodies of deceased persons with COVID-19, tissue and swab samples collected from five bodies were inspected for viral RNA by RT-qPCR and viable virus in cell culture. Specimens collected from one body were excluded from further analysis, since viral RNA was no longer detected antemortem and cell culture from specimens collected postmortem remained negative, too. Of specimens collected from remaining four bodies, viral RNA was detected in all lung tissue samples (Figure 3 b.). Additionally, tissue samples taken from a kidney in one case (ct 34.83), cerebral cortex in one (ct 36.94), duodenum in one (ct 20.99), and swabs taken from left and right hand in one case (ct 35.55, 31.87) were tested positive for viral RNA. Based on earlier observations linking low ct to cell culture infectivity, lung tissue specimens in two of four, and duodenal tissue in one case were likely to contain viral loads at in vitro infectious levels. Accordingly, virus was isolated from lung tissues, but no CPE was observed in cell culture after exposure to duodenal tissue inoculum. Here, cell culture supernatant ct was elevated at 33.34, suggesting lower viral loads than regularly observed in positive cell culture supernatant with a mean ct of 17.34. Similarly, transferring supernatant to cells for second passaging did not result in detectable viral RNA increase or CPE, indicating no viral replication in cell culture. Isolation was reattempted once unsuccessfully. Infectious lung tissue-derived inoculum ct were significantly lower than non-infectious ($p = 0.0053$, Figure 3 c.).

In conclusion, despite high loads of viral RNA, no virus was isolated from duodenal tissue. Viral RNA was detected in non-respiratory organs, isolation succeeded only from respiratory tract samples.

To collect information on viral tenacity, postmortem intervals and duration of disease were analyzed retrospectively. Postmortem intervals, i.e., the period between death and autopsy, ranged from one to 17 days, as previously described by Plenzig et al., where this data was in part also published.[84] Virus was isolated from specimens collected in autopsies taking place four- and 17-days

postmortem and that tested positive by RT-PCR 11 days ante- and two days postmortem, respectively, as opposed to 29 and 19 days antemortem in the two non-infectious cases. This adds up to shorter diagnosis to autopsy intervals in the infectious group (15 and 19 versus 30 and 29 days, Figure 3 a.). Considering high viral loads being predominantly observed during early disease[8] followed by a period of increasing virus inactivation after death, this suggests that viral load, and therefore, stage of disease at the timepoint of death determined infectivity rather than postmortem intervals alone.

In summary, samples collected from two bodies were infectious in cell culture and viable virus remained in a deceased person’s body for 17 days, offering further information on postmortem infectivity and viral tenacity.

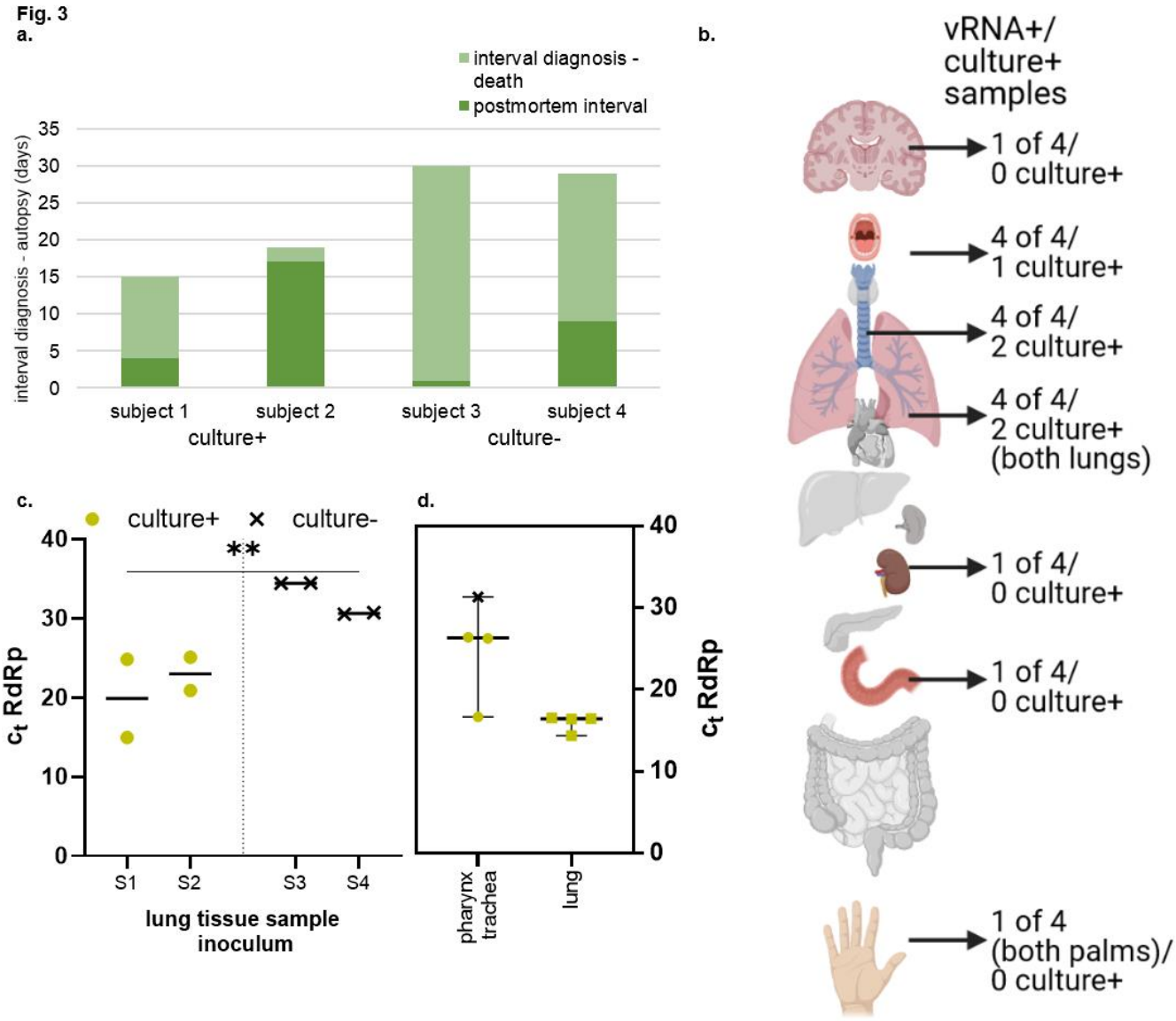

Figure 3: Postmortem virus isolation

a. *Postmortem intervals and intervals from diagnosis to death in 4 deceased individuals. Culture+ indicates virus isolation was successful from at least two specimens. Culture- indicates no viable virus was yielded from any specimen.*

b. *Organs tested for viral RNA and in cell culture: number of specimens that tested positive for viral RNA are shown on top, number of specimens positive in viral culture in bottom. Grey organs indicate no viral RNA detection.*

c. *Ct and result of viral culture are shown, culture+ meaning successful virus isolation, as opposed to culture-.*
d. *Ct and result of viral culture of two infectious individuals sorted by source site and sample type (swab versus lung tissue).*

3.1.4 Virus isolation on primary human airway epithelium

To investigate long-term viral load kinetics and cytopathic effect in a cell culture model closer to human lungs, virus isolation was attempted in parallel on Caco-2-F03 and bronchial HAE using inoculum prepared from the same sample material. In a first attempt, respiratory swab inoculum infected Caco-2-F03 cultures, i.e., viral RNA was detected in supernatant and CPE observed, but no viral RNA was detected in HAE supernatant. Therefore, isolation protocols were further aligned by increasing inoculation periods on HAE and using equal inoculum volumes, i.e., 1 mL in Caco-2-F03 medium and two times 500 µL apical inoculation for HAE. Using inoculum prepared from lung tissue, lytic CPE was complete in Caco-2-F03 after three days, no CPE was observed in HAE microscopically. Viral RNA was continuously detected in HAE supernatant for 45 days, increasing until 35 days post inoculation, despite a washing step with PBS repeated every 5 days (Figure 4 a.). Passaging of the viral isolate resulted in increasing viral RNA in HAE supernatant five days post inoculation in comparison to original isolation culture (passage one) and inoculum, peaking at passage two (Figure 4 b.). Similarly, viral RNA detected in Caco-2-F03 cell culture supernatant peaked at passage two. In passages one, two and three, viral loads started decreasing after a shorter amount of time (ten and five days, respectively).

In total, bronchial HAE cultures were able to harbor long-term infection after apical inoculation. Possible explanations for shortening periods during which increasing viral load was observed could include presence of inhibitory factors in cell culture supernatant or increased cell death due to higher viral loads in inoculum and remain to be further investigated.

Fig. 4

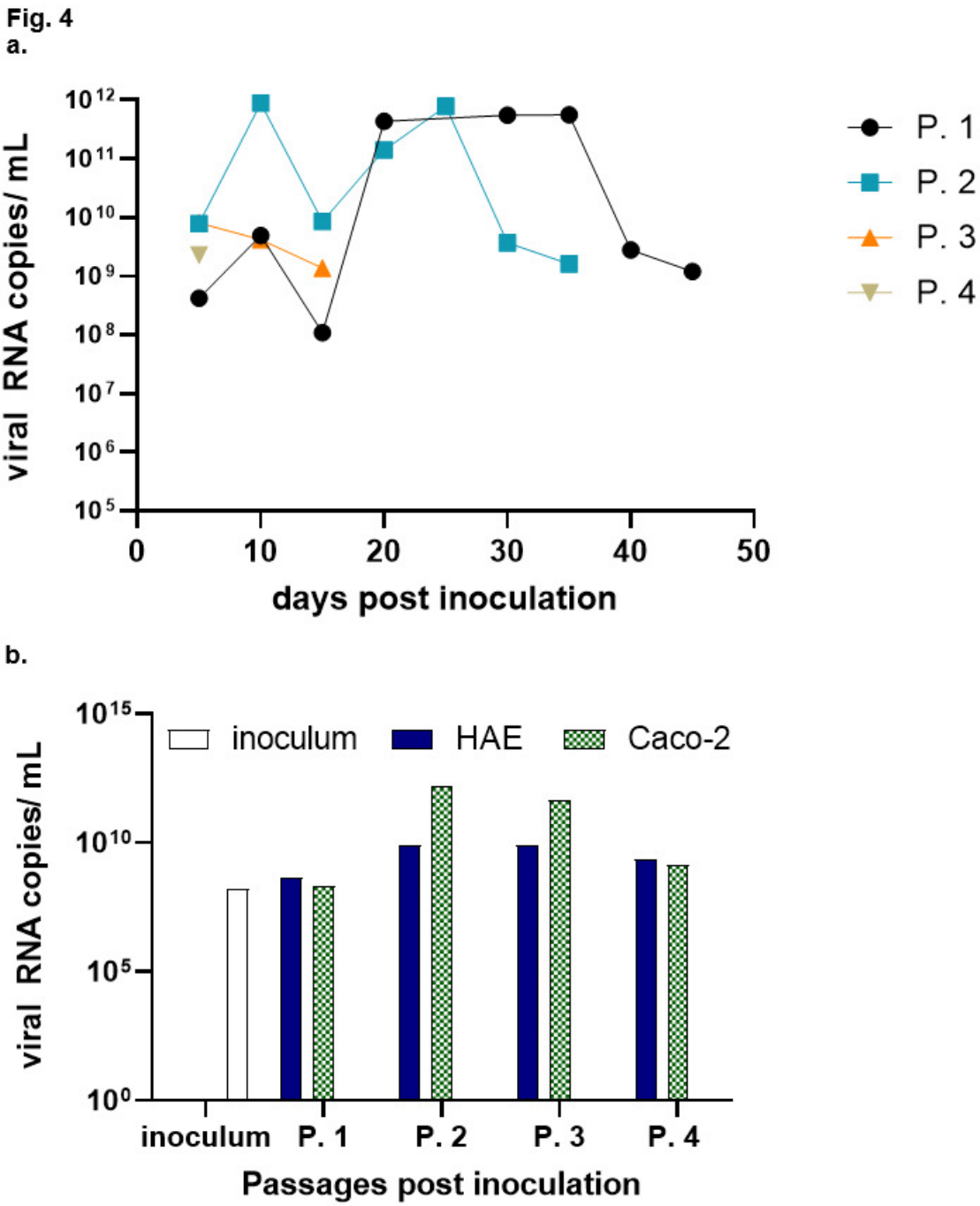

Figure 4: Virus isolation on human airway epithelium

a. Viral RNA in apical wash. Passage (P.) one to four are shown.

b. Viral RNA in apical wash versus Caco-2-F03 supernatant.

3.2 Viral replication kinetics

For characterization of potential kinetic differences in replication amongst isolates, Caco-2-F03 cells were infected at MOI one. Thereafter, supernatant was collected at three different timepoints and inspected for viral RNA by RT-qPCR. Additionally, cells were immunocytochemically stained targeting spike protein. Stained target structures were automatically counted for quantifiable results.

Spike positive area correlated with viral RNA copies at ten and 24 hours post inoculation (Spearman $r = 0.80$ at ten h p.i., $p < 0.0001$, Figure 5 a.; Spearman $r = 0.66$, $p < 0.001$ at 24 h p.i.), but not at 48 hours ($p = 0.072$, Figure 5 b.). Pronounced lytic CPE after 48 hours (Figure 5 d.) in comparison to mock (Figure 5 c.), visibly beginning at 24 hours post inoculation by light microscopy, is a plausible explanation for this poor correlation, since areas in which cell lysis is well pronounced are stained less and are not counted as spike positive area. Microscopically, at 24 hours post inoculation, staining appears homogenous across all SARS-CoV-2 isolates which is reflected in similar percentage of spike positive area and viral RNA copies per milliliter. However, quantification of staining could not detect the difference in copy numbers in SARS-CoV sample supernatants in contrast to SARS-CoV-2. This is likely inherent to the quantification method of staining, which relies on image resolution and plateaus when single stains are no longer discernible.

Therefore, quantification of immunocytochemically stained surface is an alternative to quantification by RT-qPCR only in early stages of infection, i.e., before lytic CPE forms. However, differences in viral RNA copy numbers in supernatant are likely to be underrepresented at peak timepoints.

Based on these results, variations in copy numbers after ten, 24, and 48 hours were evaluated, using immunocytochemical staining as confirmation of ten- and 24-hour timepoints. Regarding viral RNA copies in supernatant, different isolates showed high variation at ten and 48 hours post inoculation ($p < 0.0001$ for both, Figure 5 b. and e.) and minimal at 24 hours ($p = 0.0035$, Figure 5 f.). At all timepoints, SARS displayed higher copy numbers than SARS-CoV-2 isolates, suggesting more efficient replication in Caco-2-F03 cell culture.

As previously described by Toptan et al.[90], isolates three, four, six, and seven carry the now predominant D614G exchange associated with higher viral loads in vivo and in lung epithelial cell lines[93]. Focusing on the sequenced isolates FFM1 to FFM7, after ten hours larger variance was found within the D614 group (F test $p < 0.0001$ for RT-qPCR and $p = 0.0006$ for spike staining). Transformed to logarithms with equal variance, the D614 group also displayed significantly higher viral RNA copy numbers after ten hours ($p < 0.0001$, Figure 5 g.). At 24 hours post inoculation, no significant differences according to either method were observed (F test $p = 0.17$ for RT-qPCR and $p = 0.35$ for spike staining, t test $p > 0.05$, respectively). At 48 hours, variance in copy numbers was unequal between the groups (F test $p = 0.039$), transformed to logarithms with equal variances, higher viral RNA copy numbers were observed in the G614 group ($p = 0.013$, Figure 5 h.). This suggests kinetic differences of replication in Caco-2-F03 culture based on the D614G amino acid exchange. The variance may reflect the presence of further significant factors. Further research on entry, i.e. using virus with transduced spike protein in Caco-2-F03 cells would be necessary to fully ascribe the differences to the D614G exchange.

Fig. 5

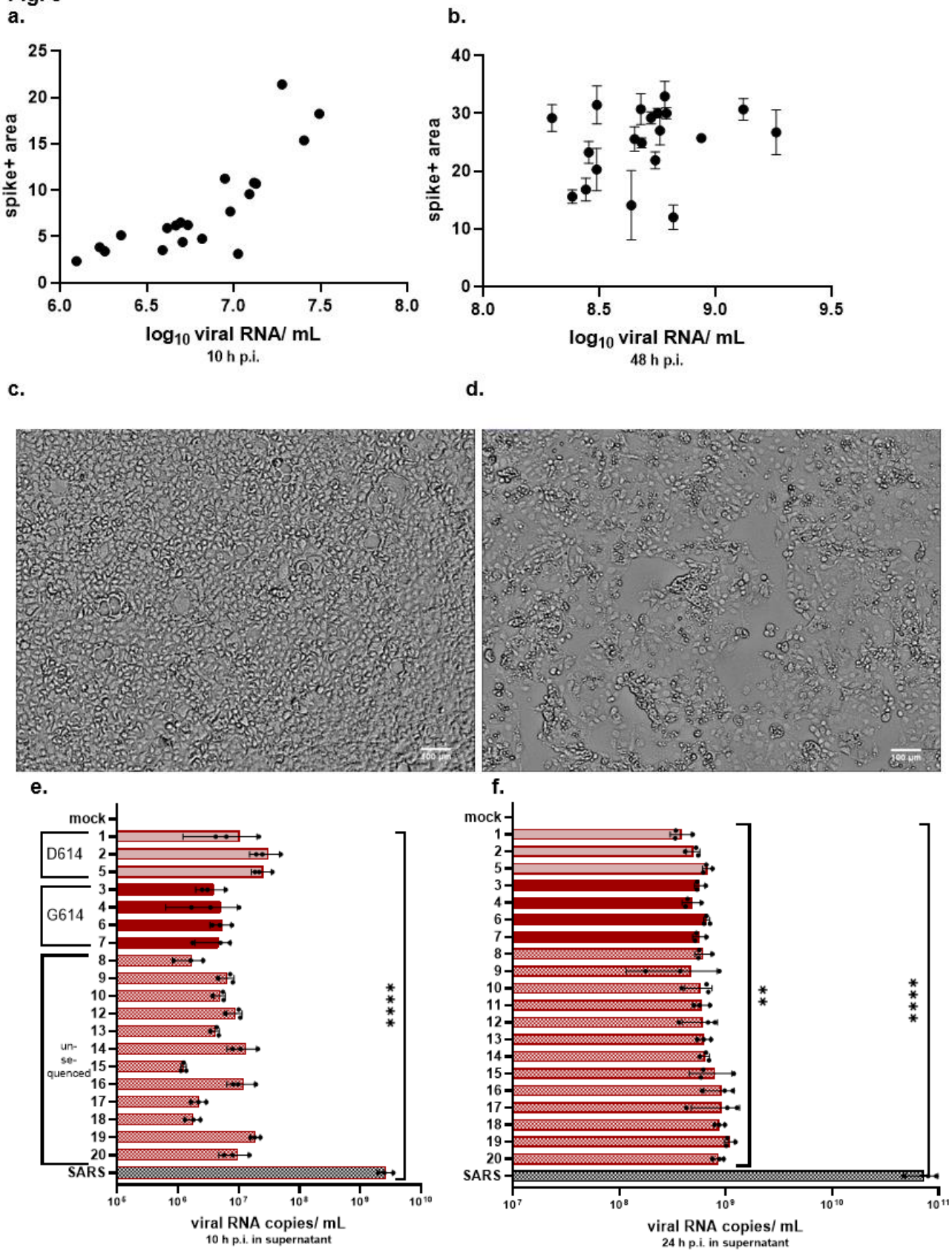
a.
spike+ area
log10 viral RNA/ mL
10 h p.i.
b.
spike+ area
log10 viral RNA/ mL
48 h p.i.
c.
d.
e.
mock
D614
G614
un-
se-
quenced
SARS
viral RNA copies/ mL
10 h p.i. in supernatant
f.
mock
SARS
viral RNA copies/ mL
24 h p.i. in supernatant

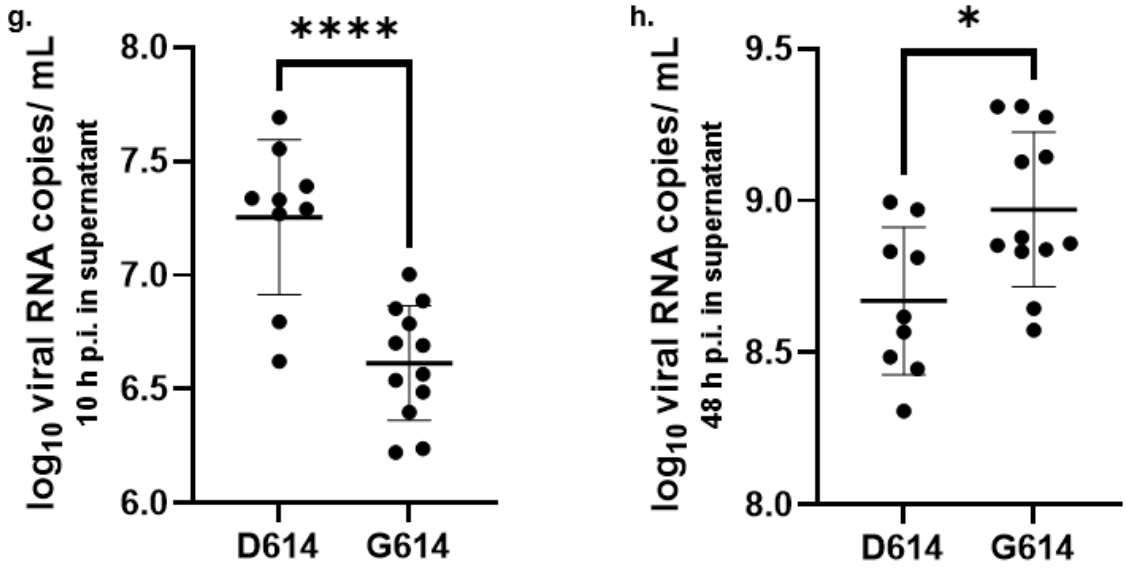

Figure 5: Viral replication kinetics

a. *Spike staining correlates with viral RNA copies at 10 h p.i.*
b. *No correlation at 48 h p.i.*
c. *Mock Caco-2-F03, scale bar indicates 100 µm.*
d. *CPE after 48 hours at MOI 0.01, scale bar indicates 100 µm.*
e. *Viral RNA copies per mililiter for 20 clinical SARS-CoV-2 isolates plus SARS at 10 h p.i.*
f. *Viral RNA copies per mililiter for 20 clinical SARS-CoV-2 isolates plus SARS at 48 h p.i.*
g. *Higher levels of viral RNA in D614 group after ten hours.*
h. *Higher levels of viral RNA in G614 group after 48 hours.*

** ; p = 0.013*

***; p = 0.0087*

*****; p < 0.0001*

3.3 Elevated Caspase 3/7 activity in presence of replicating virus

3.3.1 Caspase 3/7 activity level in different cell types

CPE was observed in Caco-2, but not in HAE cell culture. To characterize CPE and possible involvement of caspases, caspase 3 and 7 activity was measured at ten-, 24-, and 48-hour timepoints. A commercially available kit was used, modified for larger sample quantities, detecting enzyme activity based on a luminescent signal emitted after caspase 3 or 7 mediated cleavage.

By exposing viral inoculum to ten minutes of UVC-radiation and subsequent immunocytochemical double stranded RNA-staining (dsRNA), an intermediate in RNA-viral replication cycles and therefore a surrogate marker of replicating virus, a possible link between Caspase activity and the presence of replicating virus was assessed. In presence of UVC-exposed virus, dsRNA levels were comparable to mock ($p > 0.9999$, $p < 0.0001$ for non-exposed virus versus mock, Figure 6 a.). After 24 hours at a MOI of one, cell cultures inoculated with non-UVC-exposed virus showed higher caspase 3/7 activity than mock ($p < 0.0001$), while cells inoculated with UV-exposed virus and mock showed no difference ($p = 0.67$, Figure 6 b.). Within the non-UVC-exposed group, high levels of dsRNA were not correlated to elevated Caspase 3/7 activity ($p = 0.1650$, $R^2 = 0.1042$, Pearson correlation coefficient).

In conclusion, caspase 3/7 activity is elevated in the presence of replicating virus.

In a second step, caspase 3/7 activity amongst different SARS-CoV-2 isolates in Caco-2-F03 cells was compared. During UV-exposure experiments, there was some variance in caspase activity in the non-exposed group. In order to possibly explain these observed differences, viral load was correlated to caspase activity. Additionally, one SARS isolate was included for comparison after higher viral loads were detected in previous experiments.

Caspase 3/7 activity was measured after ten, 24, and 48 hours. Caspase 3/7 activity was significantly elevated in comparison to mock at all timepoints (one-

way ANOVA $p < 0.0001$, Figure 6 c.) and in all isolates (Figure 6 d.). Among infected samples, high levels of spike staining correlated positively with elevated caspases after 24 hours with immunocytochemistry-based quantification at MOI 0.01 ($p = 0.0007$, $R^2 = 0.48$, Pearson correlation for spike staining, Figure 6 e.), to a lesser extent after ten hours with RT-qPCR at MOI one ($p = 0.0495$, $R^2 = 0.1978$). In comparison to SARS-CoV-2, SARS showed lower caspase activity in relation to viral RNA copy numbers ($p = 0.0009$, Figure 6 f.).

While Caspase 3/7 activity increased with MOI (Figure 6 c.) and viral RNA copies, low R^2 suggests factors other than viral load influence caspase 3/7 activity, such as virus isolate characteristics or caspase-independent cell death, especially at high MOI. Furthermore, by measuring Caspase 3/7 activity, infected samples are discernible from mock after 10 hours, i.e., before microscopically visible CPE formation. This may facilitate laboratory workflow by shortening cell culturing time as earlier marker of infection than CPE formation.

To assess whether Caspase 3/7 activity increases in infected HAE, nasal and bronchial HAE were infected at MOI 1 and enzyme activity was measured using the same commercially available kit modified as described above. Five days post inoculation, Caspase 3/7 activity was elevated in comparison to mock (both cell types infected versus mock $p = 0.0027$; nasal: $p = 0.0015$, Figure 6 g.) and HAE displayed no microscopically visible CPE. Cultures derived from nasal epithelium tended to display higher activity in comparison to bronchial with greater variance among the samples (two-way ANOVA, Bonferroni-corrected $p = 0.02$; 95% CI nasal: 4.95 – 5.19; 95% CI bronchial: 3.67 – 5.14, Figure 6 g.), matching differences in detected apically released viral RNA ($p = 0.0076$, Figure 6 h.).

This demonstrates that elevated caspase 3/7 activity is not a Caco-2-F03-specific reaction to SARS-CoV-2 infection.

Fig. 6

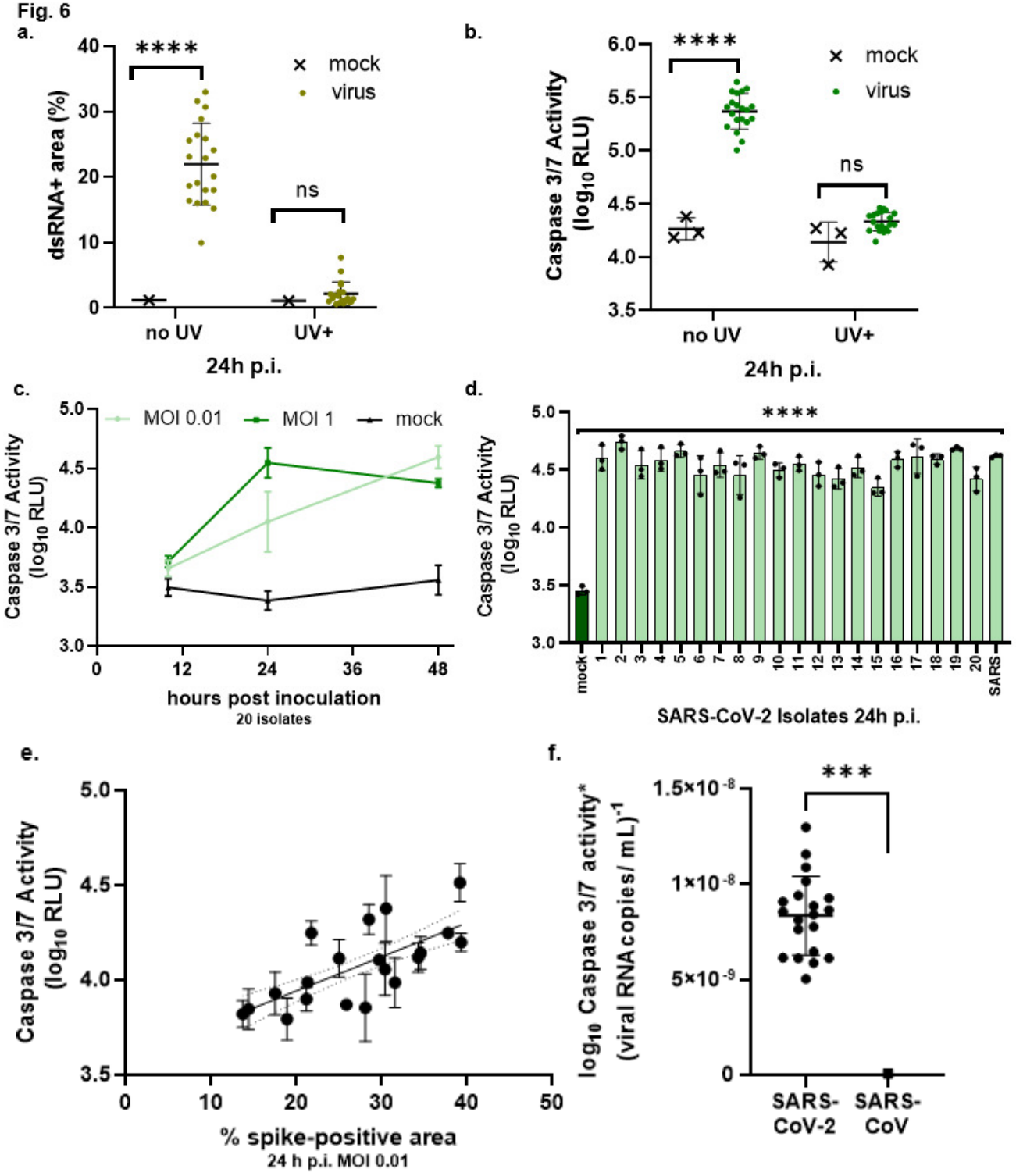
a.
dsRNA+ area (%)
****
mock
virus
ns
no UV
UV+
24h p.i.
b.
Caspase 3/7 Activity (log10 RLU)
****
mock
virus
ns
no UV
UV+
24h p.i.
c.
Caspase 3/7 Activity (log10 RLU)
MOI 0.01
MOI 1
mock
hours post inoculation
20 isolates
d.
Caspase 3/7 Activity (log10 RLU)
****
mock
SARS
SARS-CoV-2 Isolates 24h p.i.
e.
Caspase 3/7 Activity (log10 RLU)
% spike-positive area
24 h p.i. MOI 0.01
f.
log10 Caspase 3/7 activity* (viral RNA copies/ mL)-1
***
SARS-CoV-2
SARS-CoV

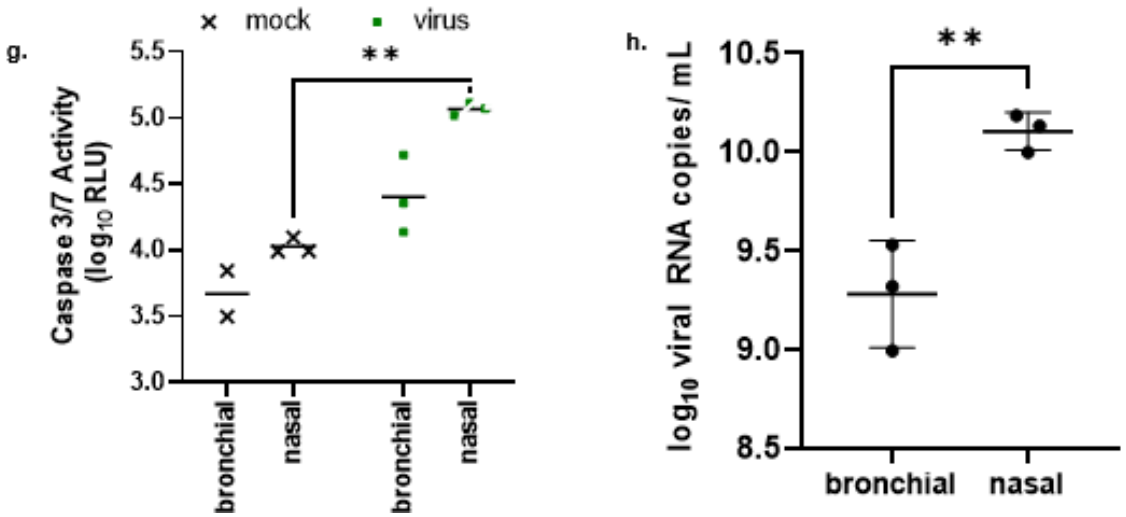

Figure 6: Elevated caspase 3/7 activity in different cell types

a. *UV-exposure inactivates SARS-CoV-2 leading to lower dsRNA levels*
b. *Presence of UV-inactivated virus does not lead to caspase 3/7 activity increase.*
c. *Mean Caspase 3/7 activity of 20 isolates over 48 hours at different MOI.*
d. *Caspase 3/7 activity is elevated in 20 clinical isolates.*
e. *Caspase 3/7 activity correlates with quantification of spike staining.*
f. *Ratio of caspase 3/7 activity to viral RNA copy number is smaller than with SARS-CoV-2.*
g. *Caspase 3/7 activity is increased in infected HAE cells of bronchial and nasal origin.*
h. *Viral RNA in apical wash in corresponding HAE.*

*****; $p < 0.0001$*

****; $p < 0.001$*

***; $p < 0.01$*

ns; non-significant, $p > 0.05$

3.3.2 Emricasan decreases CPE formation

Following the results depicting enhanced caspase 3/7 activity in infected cell cultures, the effects of caspase inhibition on CPE and virus replication were analyzed. Additionally, inhibition of mixed lineage domain like pseudokinase (MLKL) was studied, as MLKL is involved downstream of receptor-interacting serine-threonine kinase 3 (RIP3) in necroptosis.[94] Therefore, Emricasan, a small molecule pan-caspase inhibitor, and Necrosulfonamide, a MLKL inhibitor were employed in serial drug dilution assays with caspase 3/7 activity, virus replication, and CPE formation after 24 and 48 hours as endpoints with Remdesivir as additional reference. Neither Emricasan nor Necrosulfonamide displayed significant cytotoxicity as measured by MTT after 48 hours (one-way ANOVA $p = 0.5417$ for Emricasan, $p = 0.0046$ with Necrosulfonamide due to measured elevated viability in comparison to mock; Figure 7 a. and c.).

After 24 hours at MOI 0.01, no CPE was microscopically visible in treated and untreated infected cells. This aligns with previous observations using the same MOI. At higher concentrations, all compounds reduced caspase 3/7 activity to levels below or comparable to uninfected mock (one-way ANOVA $p > 0.05$ in comparison to mock for ≥ 12.5 µM Necrosulfonamide, Emricasan lower than mock for concentrations ≥ 0.63 µM, Figure 7 i. and j.). After 24 hours, virus load was reduced in presence of Remdesivir, and in higher concentrations of Necrosulfonamide and Emricasan as presented by immunocytochemical s-protein staining ($p < 0.0001$, one-way ANOVA $p = 0.0002$, $p \leq 0.0020$; Figure 7 e. and f.). After 48 hours, virus was quantified by RT-qPCR using supernatant. Here, no inhibition of viral load was observed in presence of Emricasan and Necrosulfonamide (one-way ANOVA $p = 0.44$ and $p = 0.06$, respectively, Figure 7 b. and d.). Caspase 3/7 activity in comparison to mock was elevated in presence of Necrosulfonamide (one-way ANOVA $p < 0.0001$, Figure 7 i.) and comparable or below mock-levels in presence of Emricasan (one-way ANOVA $p > 0.05$ or $p = 0.016$ below mock, Figure 7 j.). Microscopic read out of CPE showed reduced formation in presence of Emricasan only (Figure 7 g. and h.).

In summary, caspase and MLKL-inhibition reduced viral load after 24 hours, but not after 48 hours. Therefore, the effect especially in comparison to known antiviral compound Remdesivir can be deemed moderate. Caspase 3/7 activity in comparison to untreated virus control was decreased in presence of both compounds, Emricasan lowering activity more potently and consistently over 48 hours than Necrosulfonamide. CPE after 48 hours was less pronounced in wells treated with Emricasan. Hence, Emricasan could be utilized as cytoprotective compound in infected Caco-2-F03 cells despite no antiviral effect regarding replication. This may be the result of caspase inhibition, small molecule interactions, or a combination.

To objectify the findings concerning destructive CPE formation, serial drug dilution assays were conducted with Emricasan, Remdesivir, and Emricasan with Remdesivir, whereby nuclei as indicator for intact cells were identified with DAPI and viral proteins with spike-protein specific fluorescent markers allowing for automated quantification. The aim was to validate microscopically visible lytic CPE with DAPI-counts. At MOI 0.01 48 hours post inoculation, DAPI counts were lower than mock in untreated samples ($p < 0.0001$, Figure 8 d.). Accordingly, in presence of a compound and virus, DAPI counts rose in a dose-dependent manner (Figure 8 d. and f., $R^2 = 0.9428$ for Remdesivir plus Emricasan, $R^2 = 0.9763$ for Remdesivir, $R^2 = 0.6102$ for Emricasan). In presence of Remdesivir, and Remdesivir plus Emricasan, spike-protein levels were reduced ($R^2 = 0.9563$ for Remdesivir plus Emricasan, $R^2 = 0.9807$ for Remdesivir, Figure 8 e.). This was not the case with Emricasan (Figure 8 e.). Here, statistically insignificantly higher ($p = 0.1019$, Figure 8 e.) viral titers expressed in lower inhibition rates may well result from less pronounced lytic CPE and therefore longer periods of intracellular virus replication. Alone and in combination with Remdesivir, DAPI-marked cell counts increased, signifying less cell lysis and thus higher cell survival. The increase of DAPI counts paired with unchanged viral load suggest that this cytoprotective effect does not depend on viral load. In summary, Emricasan as cytoprotective and Remdesivir as antiviral compound reduced viral titers while promoting cell survival in Caco-2-F03 cells.

Fig. 7

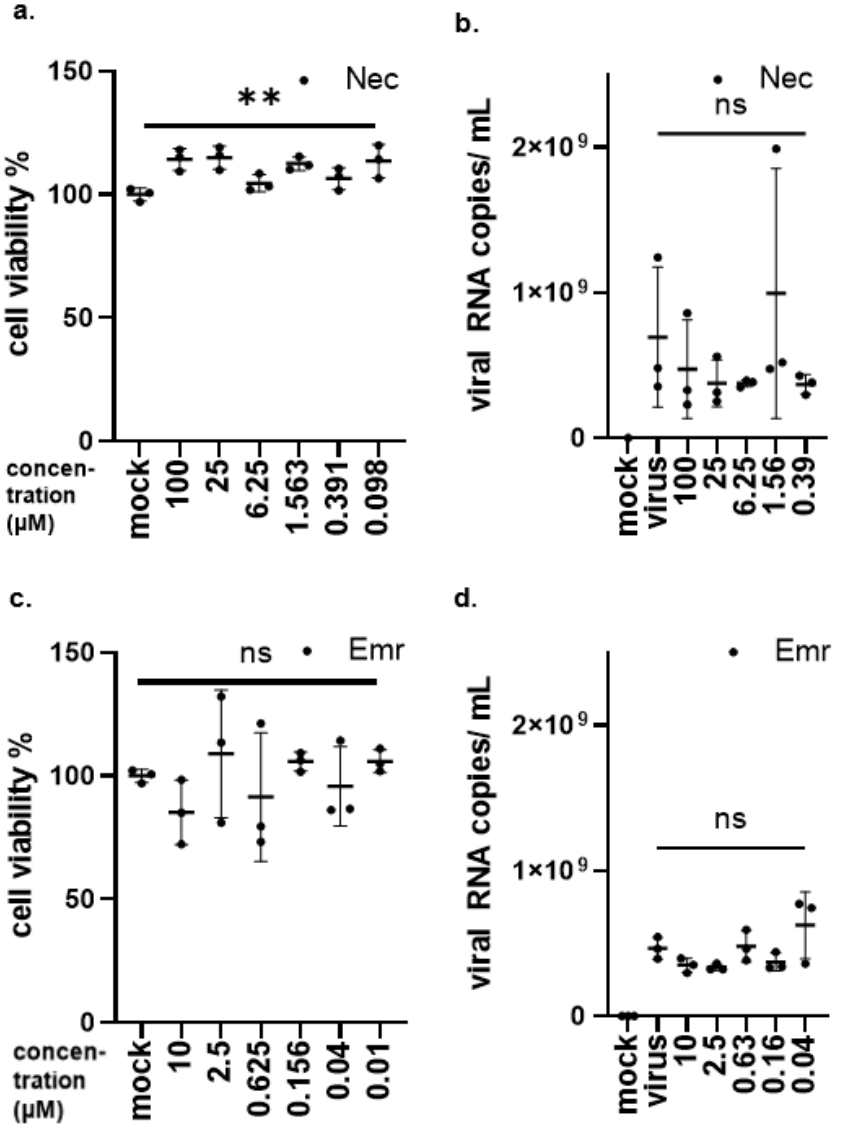

Figure 7: Emricasan and Necrosulfonamide lower caspase 3/7 activity and CPE formation at different efficiency

a. *Cell viability as measured per MTT for Necrosulfonamide.*
b. *Viral RNA in supernatant after 48 hours in presence of Necrosulfonamide plus virus.*
c. *Cell viability as measured per MTT for Emricasan.*
d. *Viral RNA in supernatant after 48 hours in presence of Emricasan plus virus.*

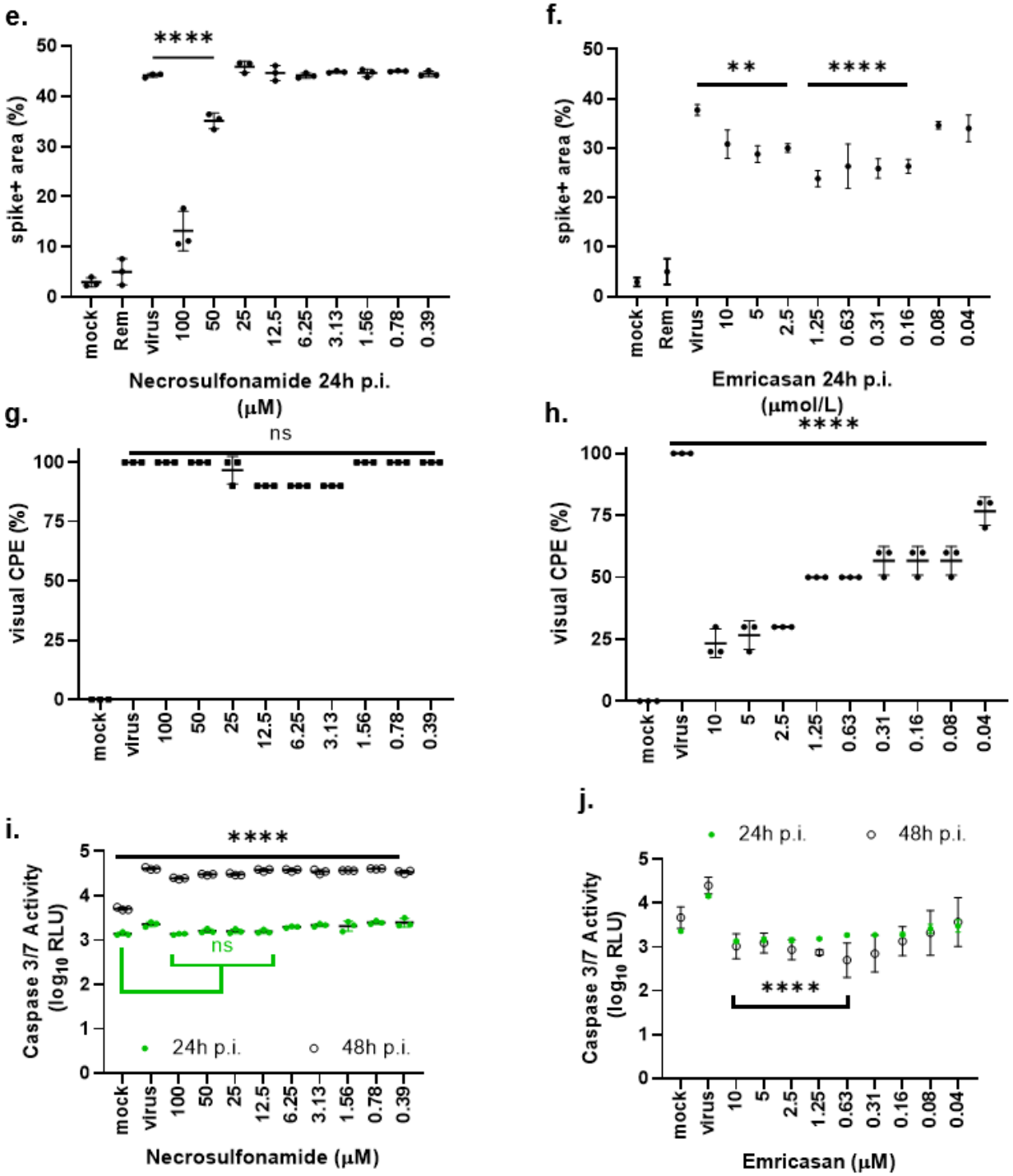

e. Spike staining after 24 hours in presence of Necrosulfonamide plus virus.

f. Spike staining after 24 hours in presence of Emricasan plus virus.

g. Visual CPE score after 48 hours for Necrosulfonamide.

h. Visual CPE score after 48 hours for Emricasan.

i. Caspase 3/7 activity after 24 and 48 hours for Necrosulfonamide.

j. Caspase 3/7 activity after 24 and 48 hours for Emricasan.

Fig. 8

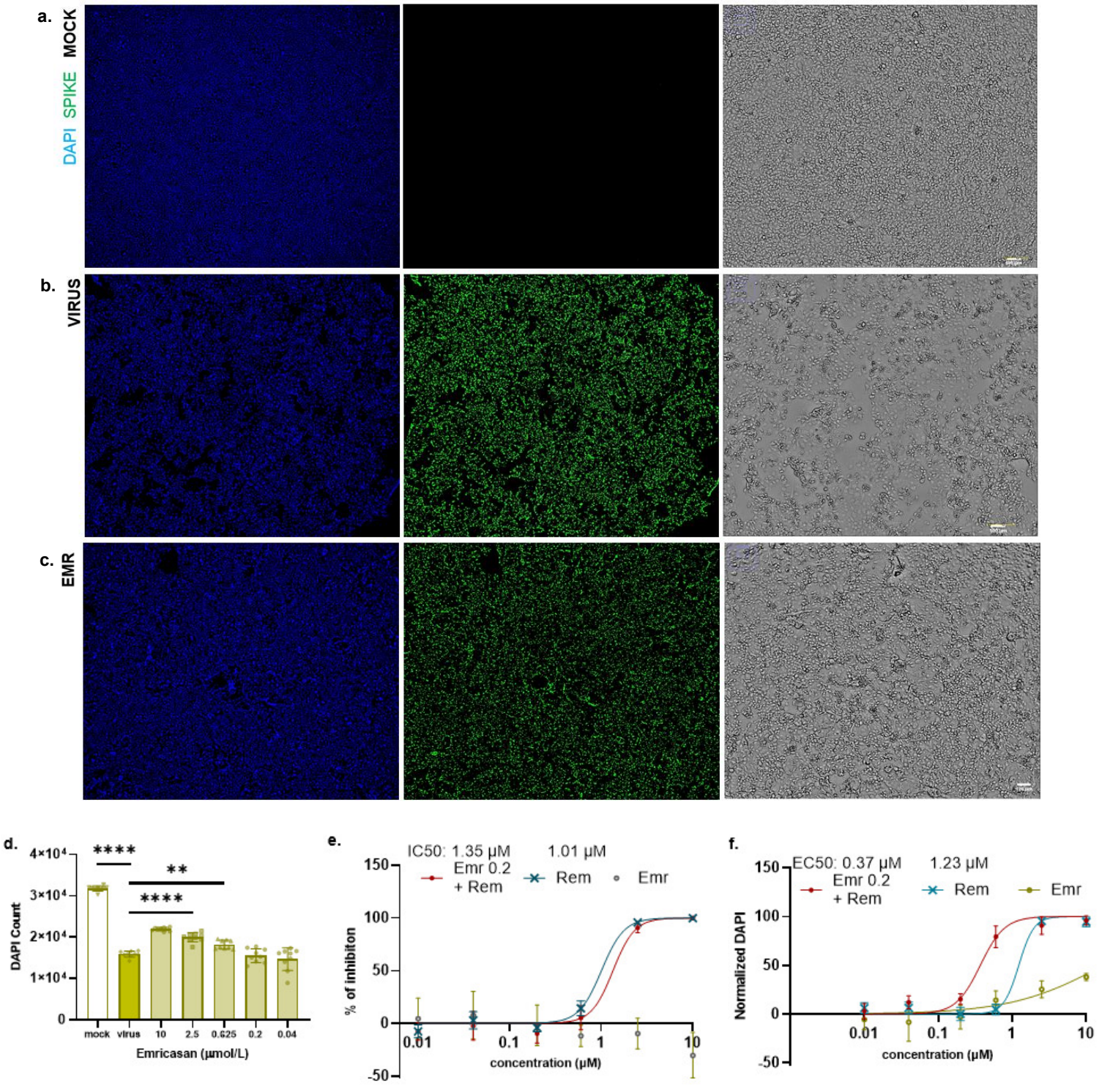

Figure 8: Emricasan increases cell survival.

a. (top row) mock: cells are at confluency as seen by blue DAPI staining. Green: spike protein.

b. (middle row) virus: CPE visualized by reduced confluency.

c. (bottom row) Emricasan (EMR) plus virus: confluency level between mock and virus, spike level comparable to virus.

d. DAPI counts in presence of Emricasan and virus.

e. Normalized inhibition curves of Remdesivir, Remdesivir plus Emricasan 0.2 µmol/ L, and Emricasan alone.

f. Normalized DAPI counts. Mock is set to 100%, virus to 0% for normalization.

*****; p < 0.0001*

***; p < 0.01*

Scale bars indicate 100 µm,pictures of wells at same magnification.

4 Discussion

4.1 Virus isolation

4.1.1 Ct-dependent infectivity

During an unprecedented pandemic, research on determinants of transmissibility was needed as guidance for public health policy decision-makers. Profiting from experience with SARS and with increasing data available, ingestion of respiratory droplets and aerosol were identified as main mode of transmission.[95,96] Droplets are commonly defined as particles with a diameter of > 5 µm, while smaller aerosol can hover and therefore contaminate air for longer periods of time.[97] Therefore, using cell culture infectivity as surrogate marker, the aim was to determine limitations of infectivity. If a maximum ct that when surpassed would no longer result in virus isolation could be identified, as in a cut-off value, then it may be possible to infer a person's potential to transmit the virus based on ct in clinical samples.

Here, a mean ct of 31.82 was detected in culture negative samples, but with some overlap to culture positive samples. Taking on the opposite perspective, when collected from the upper respiratory tract, all samples at ct 24.91 and lower were infectious in cell culture. Other research on infectivity based on data from 2020 finds a smaller range of infectivity. [8,98-100] Wölfel et al. report no virus isolation from samples at < 10^6 copies/ mL^8. At this level, all analyzed upper respiratory tract samples in this work were infectious in cell culture. Bullard et al. describe no isolation at a ct > 24 using E-gene as target.[100] However, there are reports on isolation at higher ct or lower viral load than observed here[101] and comparable ranges.[11,102] Yamada et al. used VeroE6/TMPRSS2 cells finding comparable and higher ct for infectivity in cell culture.[101]

Drawing from laboratory-based reasons for this discrepancy, different cell culture models and cell line-characteristic levels of virus susceptibility may explain the difference in range. Here, Caco-2-F03 cells were used, a subline with high ACE2 and TMPRSS2 level expression.[85] As published by Bojkova et al., this subline displayed an increased susceptibility to SARS-CoV-2 in comparison to

other cell lines, including Vero and Calu-3, and other Caco-2 cells.[85] Due to different characteristics of the cell lines used in different laboratories, it is difficult to make standardized predictions of infectivity based on viral load or ct even in vitro. On top of this, different PCR targets were used, which can also lead to different values.[103,87] With the Caco-2-F03 cell line, it could be argued that the susceptibility profile leads to overly sensitive results beyond the frame of reference determined by other commercially available cell lines that are routinely used for virus isolation. There is also the problem of reproducibility of these results as the subline is not used by many laboratories. This is especially important in the current pandemic, since public health decisions on isolation and quarantine are also, beside other research, based on in vitro infectivity studies.[104] For instance, the German federal guideline supported by the Robert Koch-Institute reported a ct of 30 as cut-off value.[6] Based on the data collected here and published in part in Toptan et al.[82] and Kohmer et al.[83], the predicted probability of virus isolation as per developed function demonstrated above at a ct of 30 is 38,4%. The absolute cut-off ct value found here is 35.26. However, cell culture as surrogate marker already constitutes a strong simplification of human-to-human transmission and cell lines with augmented receptor profiles are common.

Therefore, it can be argued that the aim of cell culture models for infectivity should be maximizing sensitivity for evidence of infectious virus rather than modeling human-to-human transmission realistically. This can be shown in epidemiological transmission studies, which can be supplemented with in vitro infectivity data. Additionally, when formulating infectivity criteria, research and decision makers may also benefit from a broader spectrum of cell culture models in use. In total, these results show that ct can be used as an additional criterion of infectivity. The overlap in values leading to different viral culture results suggest the presence of other factors, or biases, influencing infectivity. For example, early-stage disease with replicating virus could yield the same amount of detected viral RNA as a prolonged infection with no viable virus remaining, which is also in line with research finding that virus isolation success rates are highest shortly after diagnosis.[105,106,8,11,107] This also highlights the importance of virus isolation

studies, as PCR-results only inform about the presence of nucleic acids, as opposed to detection of viable virus in cell culture. Therefore, it is difficult to formulate a definitive cut-off ct value excluding infectivity and assessment of infectivity based on ct should be reported as predicted probability whenever practical circumstances allow it.

4.1.2 Specimen source site-dependent infectivity

Knowing which sample type is most likely to result in virus isolation is beneficial in clinical and research contexts. Here, samples from different parts of the body were evaluated and virus was only isolated from samples collected from respiratory tract organs. Over the course of virus isolation experiments for this thesis, data[108,8,92,106]and recommendations[109110,85,111] concerning ideal testing and respiratory sample collection for PCR changed, finding no significant evidence in favor of nasopharyngeal swabs[8], significantly higher viral loads[108] or higher sensitivity for a combination of naso- and oropharyngeal swab sampling[92,112]. In January 2020, the WHO recommended separate samples but combined transportation,[111] in March no clear preference was given,[110] and in September combined testing was cited as more sensitive[109]. Taking this into consideration, specimens that reached the laboratory labeled as “respiratory” without further specification could well be combined naso- and oropharyngeal swabs, as opposed to those labeled more precisely.

Focusing on viral culture and respiratory specimen type, there is evidence for benefits in nasopharyngeal swabs[105,113,114] and sputum[8]. First, all respiratory specimens were included. According to the data collected here with emphasis on viral culture, rather than RNA detection, and including respiratory tract specimen only, specimen source site did not significantly influence infectivity. In a second step, cases where multiple specimens were collected from the same individual were examined. Here, in one out of six cases viral culture was discordant. Importantly, the viral culture negative specimen was collected from the oropharynx, thus reflecting clinical testing standards. The clinical implications

however remain unclear, as this was a single observation within a small sample. Also, from a qualitative point of view, viral RNA was detected in all specimens which would have at least diagnosed SARS-CoV-2 presence. Another interesting observation was the BAL specimen with low ct and negative viral culture. In principle, virus isolation from BAL is possible.[115,116] Reasons for this surprising result can only be speculated, higher levels of RNA fragments are for instance imaginable.

As detection of high levels of RNA is, as discussed above, demonstrably linked to infectivity, this can be considered consistent with findings cited above that find no significant difference in sensitivity between sample source sites, bearing in mind that RNA levels do not translate to positive viral culture. Research on viral culture reports which specimen source site or sample type yielded most virus isolation, but does not evaluate this independently of other factors, such as ct or viral load and symptom onset. As presence of viral RNA and infectivity are positively linked with SARS-CoV-2, this on the one hand simply reflects the idea of higher likelihood of viable virus at sites with high viral RNA loads and can therefore lead to valid results. However, scenarios that do not follow this rationale are imaginable, e.g. different amounts of sample material or dilution. Since the specimens analyzed were not collected according to a study protocol, but simply to public health and clinical standards by a wide variety of health care professionals, differences in collection and labeling may have influenced the data. Additionally, sample size of sputum, BAL, and other lower respiratory tract specimens was very small. In total, virus was isolated from all sample source sites of the upper respiratory tract, conceptually demonstrating productive infection. Prospective studies on specimen source site and type and influence on viral culture are warranted.

4.1.3 Comparison of specimens collected postmortem

Insights into post-mortem infectivity help formulate strategies on how to handle the deceased safely. Additionally, postmortem analysis of organs can

elucidate the systemic nature of the disease. Especially when this data was collected in 2020, information on postmortem infectivity was scarce: Several sources detected viral RNA after more than a month,[117,118,46] one study reporting four months postmortem in exhumated corpses.[119] Another study detected RNA 230 days past symptom onset.[120] Postmortem infectivity has been demonstrated in cell culture[121,122,120] and possible transmission to forensic practitioners observed in two case reports.[123,124]

Here, as published in Plenzig et al.,[84] it was demonstrated that infectious virus could be found up to 17 days postmortem, a longer interval than is found in literature with up to 12 days and the longest within the examined group.[120-122] Replicating virus was found in the lower respiratory tract after relatively short duration of illness (two and nine days). Despite different length of postmortem intervals, safekeeping circumstances and temperature are likely equivalent, as three of four individuals died in hospitals. The remaining case was found the following day and cooled thereafter. Moreover, despite later cooling, this case belonged to the infectious group. Comparing the line of events of the four subjects, common characteristic of the two infectious cases was the shorter interval since diagnosis or, in one case, onset of symptoms.[84] This matches findings by Stein et al., that categorized subjects by duration of illness and found infectivity in more recent cases, all postmortem intervals being considerably shorter with a median of 22.2 h.[120] Longest duration of illness resulting in positive viral culture was 12 days[120] which, again, coincides with the longest duration here at 11 days, particularly as this interval begins with positive testing as opposed to onset of symptoms. Research on transmission support the underlying idea of increased infectivity during early disease[10], thus translating to higher levels of infectious virus remaining after death. As stated by Plenzig et al., a limitation to these findings is that no timepoint for when corpses ceased to be infectious could be given.[84] Therefore, research with consecutive sampling followed by viral culture would be valuable to determine postmortem infectivity risk. Likewise, as intervals reaching from diagnosis to autopsy also differed between the two groups, data on not infectious cases with shorter postmortem intervals could add

helpful information. Another pragmatic approach could be evaluating the individuals' last ct, if available.

Viral RNA was detected in brain (one), lung (four), kidney (one), and duodenal tissue (one), RNA-positive swabs were collected from pharynx (four), trachea (four), lungs (four), and palms of both hands (one). None was found in thyroid gland, heart, liver, spleen, pancreatic, and colon tissue. While one specimen of duodenal tissue also exhibited high viral loads, highest were found in lungs and virus was isolated only from the respiratory tract in two out of four examined subjects. While this does not demonstrate tissue tropism, it points towards involvement of non-respiratory organs. Accordingly, there is now a large body of evidence on viral RNA detection and infectivity outside of the respiratory tract, supporting the findings above and the notion of a systemic disease.[120,125,126,44,127,128] In 2020 and 2021, Stein et al. isolated virus postmortem from the jejunum, right heart ventricle, choroid and/ or sclera, adrenal gland, and mediastinal lymph nodes.[120] Extra-respiratory tract infection was demonstrated amongst others for myocardial cells,[125] different cell types of the brain,[120] liver,[129] kidneys,[127,130,131] endothelium,[132-134] and the small intestine[131] including duodenum specifically.[135,136] In a single interesting observation here, low ct was found in a duodenal tissue specimen, indicating viral RNA at levels that, as discussed above, were usually linked to successful virus isolation. Isolation was attempted twice using parts of the same specimen. As there is evidence of SARS-CoV-2 replicating in the duodenum in vivo[135] and has been isolated from the small intestine,[120] it seems plausible that preanalytical circumstances of this specimen could have reduced viable virus to a non-infectious level. Decomposition beginning in the intestine,[137] these processes could have affected infectivity. Possible reasons for high levels of viral RNA could be infection of duodenal epithelial cells[135] or presence of infected mononuclear leukocytes.[120] As the tissue was not analyzed histologically or on a single cell-level, it is not possible to further differentiate here. Further research comparing different virus variants and intestinal parts, ideally matched to the individual dispersion of gut-associated lymphoid tissue within the intestinal wall, is warranted.

In general, the findings concerning distribution of viral RNA with methods used here could be explained by reasons other than infection, i.e. postmortem decomposition of anatomical barriers and compartments and contamination or viraemia.[133,120,138] Another limitation is that the individuals were not vaccinated, and infection occurred with an earlier variant. Nevertheless, as postmortem infectivity research with viral culture is scarce, the information on prolonged infectivity could still be of interest for future guidelines.

4.1.4 Specimens collected from skin and environment

Following the results of postmortem infectivity and reports of successful isolation from feces[139] and surfaces[140], thus giving rise to concerns about alternative transmission routes, the aim was to evaluate infectivity of skin and close contact surfaces in a case study, as well as a limited number of masks and filters used during ventilation.

Here, no virus was isolated from patient skin and patient environment, viral RNA was detected with ct > 36. At this level, no virus isolation was observed. Therefore, the result was in line with expectations. In this case, there was no evidence of infectivity. However, virus isolation also failed from the nasopharyngeal specimen. This is a limitation, as this individual could have simply not been infectious at this timepoint. Nonetheless, no evidence of prolonged infectivity surmounting respiratory tract infectivity was found, especially concerning the rectal swab.

No viral RNA was detected in used filters and masks. As proof-of-principle to ensure that the protocol was fit to solubilize virus on filters and test virus stability, three filters were prepared with known $TCID_{50}$/ mL titers. Here, high levels of RNA and successful virus isolation resulted from three prepared filters with ultracentrifuged virus diluted in PBS. From 24 to 48 hours ct increased, indicative of about a halving of detectable viral RNA. Likewise, van Doremalen et al. demonstrated infectivity after up to 72 hours on plastic using inoculum with 10^5 $TCID_{50}$/ mL (ct 22).[140] The results collected for this dissertation are limited by

small sample size, no data on patients or individuals wearing masks, larger drop size than potentially produced during ventilation and mismatch between saliva and PBS as diluting agent. While a protein-rich environment has been shown to increase viral stability for SARS,[141] neutralizing or inactivating factors, such as Ig-A,[142,143] could decrease stability. Also, plastic tubes used during ventilation that are closer to the patient were not tested. This demonstrates that viable SARS-CoV-2 could in principle persist on filters used during ventilation. In this small sample, there was no evidence for viable virus persisting on used filters and masks and patient environment.

4.1.5 Virus isolation on human airway epithelium

Following isolation from clinical specimens in Caco-2-F03 cell culture, isolation was also attempted in a model closer to human lungs using primary human bronchial airway epithelium in air-liquid-interface culture as reported by Bojkova et al.[144] following previous description by van Wetering et al.[145] SARS-CoV-2 infection had been demonstrated for up to 7 days.[146] Here, productive infection from a clinical specimen using apical inoculum could be demonstrated and maintained over 45 days. Apical reinfection after virus passaging was also possible. In direct comparison to Caco-2-F03 cells that exhibited extensive CPE that was microscopically beginning to be visible after one day and complete after two to maximum three days, HAE showed no visible CPE. SARS-CoV-2 exhibiting different cell line-dependent entry pathways and adapting to cell culture,[147-151] while passaging has reportedly changed entry preferences of human coronaviruses in comparison to wild-type[152,153], isolation from clinical specimens on HAE offers the possibility to work with an isolate presumably less adapted to cell culture and closer to wild-type. Also, this shows that HAE could be used for modeling of prolonged infection.

4.2 Kinetic differences between isolates

After isolating virus from clinical specimens, 20 were propagated in Caco-2-F03 cell culture for further characterization. The aim was to gather information on replication kinetics and compare isolates. The data collected here was in part published in Bojkova et al. reporting productive infection and CPE formation with all isolates, thus in support of Caco-2-F03 as cell culture model.[85] Propagation of the clinical isolates resulted in the same lytic CPE and was confirmed by RT-qPCR and immunocytochemistry, thus adhering to Koch's postulates. Higher levels of SARS-RNA in comparison to SARS-CoV-2 were detected at all timepoints. In theory, this could be an artefact due to cell culture adaptation of the SARS isolate.[153,152] However, Caco-2-F03 expressing high levels of TMPRSS2,[85] thus supporting a pathway preferred by wild-type coronaviruses, the pronounced difference seems unlikely. Moreover, the SARS isolate in question was isolated in house in Frankfurt and has therefore presumably not been passaged as frequently.[154] Ozono et al. compared lentiviruses pseudotyped with SARS and SARS-CoV-2 spike finding more efficient entry into cells expressing ACE2 plus TMPRSS2 or ACE2 alone with SARS-spike and higher TMPRSS2-dependency of SARS-CoV-2.[155] Lastly, Chu et al. observed the same after 120 hours using Caco-2 cells.[156]

The transient higher levels of viral RNA in D614 versus G614 isolates after ten hours could be indicative of advantages during early infection that are then mitigated or even reversed later on. Similarly, the smaller variance within the G614 group could on a very small scale reflect convergence. The D614G exchange is associated with higher infectivity and lower ct in humans and has replaced the original D614 spike variant.[29,157,93] It was also shown to increase infectivity in multiple cell lines independently of other non-spike mutations[20] and favors an open conformational state promoting ACE2 interaction.[21] Prevalence of syncytia formation thought to facilitate spread of infection was also higher with G614 spike than with D614.[158-160] Therefore, early temporal advantages of D614 were unexpected. In terms of more efficient spread, Rajah et al. demonstrated that syncytia formation was more prevalent in Caco-2 transfected with D614G-

spike than with Wuhan-spike after 18 hours.[158] Therefore, it is possible that after ten hours, the advantageous syncytia formation had not taken place yet, while at later timepoints with increasing formation the G614 isolates outperformed D614 carriers. However, this does not explain early higher RNA levels in the D614 group. Focusing on the possibility of more efficient entry, Bojkova et al. showed that in A549-ACE2 cells, the percentage of infected cells was higher in D614 than in G614 isolates.[85] With low levels of TMPRSS2 expressed in A549-ACE2 cells, this is evocative of TMPRSS2 involvement as a possible explanation, i.e. less dependence during entry. In Vero E6 cells also lacking TMPRSS2, this defect was not seen, speaking against this idea.[161] Further research is needed to clarify this early phase lead. In total, productive infection for 48 hours at MOI one and lytic CPE was demonstrated using isolates from clinical specimens.

4.3 Elevated caspase 3/7 activity in presence of replicating virus

Caspase 3/7 activity was elevated in presence of replicating virus and in an MOI dependent manner. This was reproduced at different timepoints and with 20 clinical isolates. Elevated levels were measurable before CPE became visible. This can be used as drug screening platform, as demonstrated by Bojkova et al. adapted to large quantities, and parts of the data presented here were also used in this publication.[85] At MOI one, there was no correlation between viral RNA or spike staining and caspase 3/7 activity, but at MOI 0.01, spike staining and caspase 3/7 activity were positively linked. It could therefore be discussed whether caspase 3/7 activity is more dependent on the presence of spike protein and therefore these levels correlate positively, while RdRp-gene copy numbers do not. However, Bojkova et al. found correlation of RdRp-gene copies and caspase 3/7 activity at MOI 0.01.[85] Additionally, the UV-exposure experiments described above also suggest otherwise, as caspase 3/7 activity in cells in presence of UV-exposed virus was comparable to mock-levels and UV-exposure does not significantly impact spike protein structure.[162,163] In conclusion, it is more likely that in this setting high MOI is accountable for the mismatch rather than

spike versus actual virus replication as measured by RdRp copy numbers. High MOI results in higher cell stress, increasing the level of cytotoxicity, possibly causing more unspecific cell reactions and artefacts. Nonetheless, one study found spike protein to induce pyroptosis in Caco-2 cells with NLRP3 inflammasome and elevated caspase 1 activity. Thus, additional research on spike protein pathogenicity in Caco-2 cells is warranted.

Viral proteins ORF3a and M in both SARS and SARS-CoV-2 can induce caspase-dependent apoptosis.[164-166] To study caspase 3/7 activity in a non-cancer cell culture model closer to the human lung, HAE of bronchial and nasal origin in ALI-culture were used. Five days after apical inoculation and infection, elevated caspase 3/7 activity levels were detected. Caspase 3/7 activity matched apical viral RNA levels with nasal epithelial cells in the lead. Higher apical titers in nasal HAE were also described by Pizzorno et al. after 48 hours, but no longer after 96.[167] Due to likely fluctuation, it is not possible to deduct general higher apical release rates for nasal-originated cells from this finding. However, this snapshot supports the relation of replicating virus and caspase 3/7 activity. In both cell systems, no CPE was observed. Lack of CPE paired with elevated caspase activity was also described by Bojkova et al. in bronchial cells, additionally finding no drop in transepithelial electric resistance, thus objectifying the finding.[85]

In line with the observed elevated caspase activity, apoptotic bronchial and nasal epithelial cells were found in SARS-CoV-2-challenged hamsters.[168] Signs of apoptosis were also present postmortem in type I and II alveolar cells, in one case with elevated caspase 3 levels collocated to spike-positive cells.[169,170] Elevated caspase 3/7 activity was also found in patients' red blood cells and non-specifically to Covid-19 in patients with ARDS.[70,80] In general, as a host cell response, undergoing apoptosis can limit viral infection, but viral interaction with apoptotic pathways can also lead to more efficient spread.[65,63] Traditionally seen as executioner caspases in apoptosis, caspase 3 can also be involved in other forms of programmed cell death, with programmed cell death pathways no longer thought of as taking place discretely, but rather in an overlapping fashion, e.g., PANoptosis, as also proposed in Covid-19.[171,172] Another example of non-

apoptotic caspase 3 involvement is GSDME-mediated pyroptosis and regulation by GSDMD degradation.[173] In immortalized bronchial epithelial cells infected with SARS-CoV-2, caspase 3 and 8 activity was shown to induce apoptosis and pyroptosis.[174] Thus, there is evidence of caspase 3 activity involvement in inflammatory and non-inflammatory pathways, resulting in different levels of tissue disruption. The detection of higher caspase 3/7 activity in infected human airway epithelium and in lung tissue demonstrates that this is not a finding unique to Caco-2-F03 cells. Differences in CPE formation with elevated caspase 3/7 activity is indicative of involvement in different pathomechanistic pathways leading to cell destruction depending on cell type and warrants further investigation.

Additionally, Covid-19 being described as a respiratory disease that can take on different levels of severity, including ARDS, not finding CPE in a respiratory tract cell model was slightly unexpected. However, in postmortem examinations, inflammation and cell damage in bronchi and bronchioli was present but moderate in comparison to the alveoli, contrary to infection patterns.[43,47] This suggests that the cell morphology observed here and by others[146] can be considered an adequate reflection of in vivo conditions. Nonetheless, further research in alveolar cell culture models is needed.

4.4 Pan-caspase inhibitor reduces CPE

Considering the diverse engagement of caspases, it is conceivable that inhibition would affect viral replication and CPE. Here, Emricasan did not affect replication but promoted cell survival while inhibiting caspase 3/7 activity. This data and finding was in part also published in Bojkova et al.[85] Additionally, MLKL-inhibition by Necrosulfonamide did not inhibit CPE formation or virus replication after 48 hours in Caco-2-F03 cells. In contrast, Remdesivir inhibited replication, CPE formation and consequently, caspase activity. This suggests that CPE in Caco-2-F03 cells is more dependent on caspase-3/7 activity than MLKL-mediated necroptosis. It also shows that while replicating virus leads to caspase

activity, replication is independent of caspase activity in this model. Due to merely incomplete CPE inhibition despite pan-caspase inhibition, demonstrated in part for caspases 3 and 7 at mock-level activity, it can be assumed that caspase-independent cell death occurs.

Cytoprotective effects during RNA-viral infection were described for Emricasan, a small-molecule pan-caspase inhibitor, in Zika-infected human neural progenitor cells while also not affecting replication.[79] In patients with chronic hepatitis C, HCV-RNA levels were again unchanged while aminotransferase levels decreased.[71] Originally developed for treatment of chronic liver diseases where excessive hepatocyte apoptosis is thought to contribute to pathogenesis,[72] it has demonstrably inhibited recombinant SARS-CoV-2 main protease Mpro.[175] In presence of Emricasan, elevated caspase activity was reduced in peripheral blood cells collected from individuals infected with SARS-CoV-2.[80] Consequences of caspase inhibition by Emricasan were however not studied. Additionally, an AI-based drug repurposing screen predicted high affinity for ACE2.[176] However, here, viral load was not reduced as seen with other Mpro inhibitors both in vitro and, in the case of Nirmatrelvir, also in patients.[177,178] On the contrary, slight increases of viral load were observed at low concentrations, possibly reflective of higher cell survival, that were mitigated in presence of Remdesivir. In combination with Remdesivir, promotion of cell survival was more efficient than with Remdesivir alone, reflected in a lower EC50, while viral load was not significantly changed. This suggests that promotion of cell survival with Emricasan is not based on antiviral activity in the sense of inhibiting replication. The demonstration of increased cell survival as opposed to demonstration of caspase activity reduction alone with no examination of cell morphology thereafter also adds value to the results shown here. As combination of Remdesivir and Emricasan lead to higher cell survival without increasing viral load, addition of a cytoprotective agent to an antiviral therapy regimen could be a useful strategy to prevent tissue damage,[79] especially as antiviral treatment in practice is limited to the early replicative phase for significant improvement of outcome.[177] However, extensive research is needed on the combination of compounds, in particular with apoptotic pathways in order to not impede

physiological host defense mechanisms.[65] A limiting factor is the cancerous origin of the used cell line. As discussed above, signs of increased caspase activity in patients warrants further research on possible cytoprotective effects of caspase inhibition.[80,97,170,169] Since Emricasan is a pan-caspase inhibitor and inflammatory and non-inflammatory pathways could lead to the detected caspase 3/7 activity increase,[171,172] further research is needed to elucidate relevant pathomechanisms.

Treatment with Necrosulfonamide, a MLKL inhibitor, did not significantly alter viral load, nor inhibit CPE formation. MLKL is involved in necroptosis and Caco-2 cells express MLKL as well as upstream mediators RIP1 and RIP3.[94,179] Necroptosis has also been shown to occur upon infection in Caco-2, and postmortem beside apoptosis in human lungs of SARS-CoV-2 patients.[179,180] Although programmed, necroptosis results in inflammatory loss of membrane integrity caused by oligomerized MLKL forming transmembrane pores. [179,181,182] It is commonly regarded as an option to contain infection when caspases are inhibited by pathogens, but MLKL is also involved in non-necroptotic functions, and connections to, as well as simultaneous occurrence of other programmed cell death pathways exist.[183-185] The membrane rupture causes not only causes inflammation and tissue damage, but can also facilitate viral spread, thus, necroptosis can both benefit and harm the host.[186] Due to pathways merging at MLKL, it's inhibition is an interesting target for evaluation of necroptosis.[187] Caspase 8 regulates necroptosis, inhibition of caspase 8 increasing necroptotic cell death.[188] The unchanged CPE and viral load suggest that necroptosis is not a predominant cell death in infected Caco-2-F03 cells. Elevated caspase activity, specifically also caspase 8,[85] support this. As viral load was reduced after 24 hours, but not after 48, it is possible that at this early timepoint, necroptosis inhibition reduced viral spread. For instance, with uninfected treated cells displaying slightly higher viability, it is possible that Necrosulfonamide has cytoprotective faculties unrelated to viral infection that initially reduce viral spread by extending maintained cell integrity at 24-, but no longer at 48-hour timepoints. While the MTT assay result for cell viability may have been influenced by the compound and the slight increase should not be overinterpreted, one study

demonstrated Necrosulfonamide reducing cell damage in neurons.[189,190] Another option could be pyroptosis inhibition through gasdermin D binding.[191] Additional research is necessary to elucidate the prevalence of necroptosis in models reflective of lung physiology.

Taken together, cell survival in presence of Emricasan was higher, indicative of caspase involvement in CPE formation.

5 References

1. Johns Hopkins Coronavirus Resource Center. COVID-19 Map - Johns Hopkins Coronavirus Resource Center. Published March 15, 2023. Accessed April 2, 2023. https://coronavirus.jhu.edu/map.html
2. Zhou P, Yang X-L, Wang X-G, et al. A pneumonia outbreak associated with a new coronavirus of probable bat origin. *Nature*. 2020;579(7798):270-273. doi:10.1038/s41586-020-2012-7
3. Li Z, Chen Q, Feng L, et al. Active case finding with case management: the key to tackling the COVID-19 pandemic. *Lancet (London, England)*. 2020;396(10243):63-70. doi:10.1016/S0140-6736(20)31278-2
4. Maier BF, Brockmann D. Effective containment explains subexponential growth in recent confirmed COVID-19 cases in China. *Science*. 2020;368(6492):742-746. doi:10.1126/science.abb4557
5. WHO. Criteria for releasing COVID-19 patients from isolation. https://www.who.int/publications/i/item/criteria-for-releasing-covid-19-patients-from-isolation
6. RKI - Coronavirus SARS-CoV-2 - Empfehlungen zu Isolierung und Quarantäne bei SARS-CoV-2-Infektion und -Exposition, Stand 2.5.2022. Published March 23, 2023. Accessed March 23, 2023.
7. Basile K, McPhie K, Carter I, et al. Cell-based Culture Informs Infectivity and Safe De-Isolation Assessments in Patients with Coronavirus Disease 2019. *Clinical infectious diseases : an official publication of the Infectious Diseases Society of America*. 2021;73(9):e2952-e2959. doi:10.1093/cid/ciaa1579
8. Wölfel R, Corman VM, Guggemos W, et al. Virological assessment of hospitalized patients with COVID-2019. *Nature*. 2020;581(7809):465-469. doi:10.1038/s41586-020-2196-x
9. Hakki S, Zhou J, Jonnerby J, et al. Onset and window of SARS-CoV-2 infectiousness and temporal correlation with symptom onset: a prospective, longitudinal, community cohort study. *Lancet Respir Med*. 2022;10(11):1061-1073. doi:10.1016/S2213-2600(22)00226-0

10. He X, Lau EHY, Wu P, et al. Temporal dynamics in viral shedding and transmissibility of COVID-19. *Nat Med*. 2020;26(5):672-675. doi:10.1038/s41591-020-0869-5
11. Arons MM, Hatfield KM, Reddy SC, et al. Presymptomatic SARS-CoV-2 Infections and Transmission in a Skilled Nursing Facility. *N Engl J Med*. 2020;382(22):2081-2090. doi:10.1056/NEJMoa2008457
12. V'kovski P, Kratzel A, Steiner S, Stalder H, Thiel V. Coronavirus biology and replication: implications for SARS-CoV-2. *Nat Rev Microbiol*. 2021;19(3):155-170. doi:10.1038/s41579-020-00468-6
13. Zhao X, Ding Y, Du J, Fan Y. 2020 update on human coronaviruses: One health, one world. *Med Nov Technol Devices*. 2020;8:100043. doi:10.1016/j.medntd.2020.100043
14. Malone B, Urakova N, Snijder EJ, Campbell EA. Structures and functions of coronavirus replication-transcription complexes and their relevance for SARS-CoV-2 drug design. *Nat Rev Mol Cell Biol*. 2022;23(1):21-39. doi:10.1038/s41580-021-00432-z
15. Ferreira G, Santander A, Savio F, Guirado M, Sobrevia L, Nicolson GL. SARS-CoV-2, Zika viruses and mycoplasma: Structure, pathogenesis and some treatment options in these emerging viral and bacterial infectious diseases. *Biochim Biophys Acta Mol Basis Dis*. 2021;1867(12):166264. doi:10.1016/j.bbadis.2021.166264
16. Lamers MM, Haagmans BL. SARS-CoV-2 pathogenesis. *Nat Rev Microbiol*. 2022;20(5):270-284. doi:10.1038/s41579-022-00713-0
17. Jones AN, Mourão A, Czarna A, et al. Characterization of SARS-CoV-2 replication complex elongation and proofreading activity. *Sci Rep*. 2022;12(1):9593. doi:10.1038/s41598-022-13380-1
18. Smith EC, Blanc H, Surdel MC, Vignuzzi M, Denison MR. Coronaviruses lacking exoribonuclease activity are susceptible to lethal mutagenesis: evidence for proofreading and potential therapeutics. *PLOS Pathogens*. 2013;9(8):e1003565. doi:10.1371/journal.ppat.1003565
19. Updated working definitions and primary actions for SARSCoV2 variants. Published March 16, 2023. Accessed April 2, 2023.

https://www.who.int/publications/m/item/updated-working-definitions-and-primary-actions-for--sars-cov-2-variants

20. Daniloski Z, Jordan TX, Ilmain JK, et al. The Spike D614G mutation increases SARS-CoV-2 infection of multiple human cell types. *eLife Sciences Publications, Ltd.* Published February 11, 2021. Accessed March 29, 2023. https://elifesciences.org/articles/65365.
21. Mansbach RA, Chakraborty S, Nguyen K, Montefiori DC, Korber B, Gnanakaran S. The SARS-CoV-2 Spike variant D614G favors an open conformational state. *Sci Adv*. 2021;7(16). doi:10.1126/sciadv.abf3671
22. Lau S-Y, Wang P, Mok BW-Y, et al. Attenuated SARS-CoV-2 variants with deletions at the S1/S2 junction. *Emerg Microbes Infect*. 2020;9(1):837-842. doi:10.1080/22221751.2020.1756700
23. Chaudhry MZ, Eschke K, Hoffmann M, et al. Rapid SARS-CoV-2 Adaptation to Available Cellular Proteases. *J Virol*. 2022;96(5):e0218621. doi:10.1128/jvi.02186-21
24. Peacock TP, Goldhill DH, Zhou J, et al. The furin cleavage site in the SARS-CoV-2 spike protein is required for transmission in ferrets. *Nat Microbiol*. 2021;6(7):899-909. doi:10.1038/s41564-021-00908-w
25. Cdc. Cases, Data, and Surveillance. Published June 3, 2023. Accessed June 3, 2023. https://www.cdc.gov/coronavirus/2019-ncov/covid-data/investigations-discovery/hospitalization-death-by-age.html
26. Yong SJ, Liu S. Proposed subtypes of post-COVID-19 syndrome (or long-COVID) and their respective potential therapies. *Reviews in Medical Virology*. 2022;32(4):e2315. doi:10.1002/rmv.2315
27. Smith DJ, Hakim AJ, Leung GM, et al. COVID-19 Mortality and Vaccine Coverage - Hong Kong Special Administrative Region, China, January 6, 2022-March 21, 2022. *MMWR. Morbidity and mortality weekly report*. 2022;71(15):545-548. doi:10.15585/mmwr.mm7115e1
28. Iuliano AD, Brunkard JM, Boehmer TK, et al. Trends in Disease Severity and Health Care Utilization During the Early Omicron Variant Period Compared with Previous SARS-CoV-2 High Transmission Periods - United States,

December 2020-January 2022. *MMWR. Morbidity and mortality weekly report*. 2022;71(4):146-152. doi:10.15585/mmwr.mm7104e4

29. Korber B, Fischer WM, Gnanakaran S, et al. Tracking Changes in SARS-CoV-2 Spike: Evidence that D614G Increases Infectivity of the COVID-19 Virus. *Cell*. 2020;182(4):812-827.e19. doi:10.1016/j.cell.2020.06.043
30. Scherr J. Pathophysiologie von COVID-19 und deren mögliche Bedeutung für Long-COVID. *Sports Orthopaedics and Traumatology*. 2021;37(3):205-213. doi:10.1016/j.orthtr.2021.08.002
31. Boscolo-Rizzo P, Borsetto D, Fabbris C, et al. Evolution of Altered Sense of Smell or Taste in Patients With Mildly Symptomatic COVID-19. *JAMA Otolaryngol Head Neck Surg*. 2020;146(8):729-732. doi:10.1001/jamaoto.2020.1379
32. John C Marshall, Srinivas Murthy, Janet Diaz, et al. A minimal common outcome measure set for COVID-19 clinical research. *The Lancet Infectious Diseases*. 2020;20(8):e192-e197. doi:10.1016/S1473-3099(20)30483-7
33. Zhu Z, Lian X, Su X, Wu W, Marraro GA, Zeng Y. From SARS and MERS to COVID-19: a brief summary and comparison of severe acute respiratory infections caused by three highly pathogenic human coronaviruses. *Respir Res*. 2020;21(1):224. doi:10.1186/s12931-020-01479-w
34. Griffin D. COVID-19: Using the Right Tools at the Right Time. *MRAJ*. 2022;10(8). doi:10.18103/mra.v10i8.3041
35. DGPI: Deutsche Gesellschaft für Pädiatrische Infektiologie. Stellungnahme der DGPI, API, DGKJ, DGPK, GPOH, GKJR, GPP und STAKOB zur Klinik, Diagnostik und Therapie von Kindern mit COVID-19 (Stand 14.02.2022). Published June 4, 2023. Accessed June 4, 2023. https://dgpi.de/klinik-diagnostik-therapie-kinder-mit-covid-feb-2022/
36. Soriano JB, Murthy S, Marshall JC, Relan P, Diaz JV. A clinical case definition of post-COVID-19 condition by a Delphi consensus. *The Lancet Infectious Diseases*. 2022;22(4):e102-e107. doi:10.1016/S1473-3099(21)00703-9
37. Helms J, Kremer S, Merdji H, et al. Delirium and encephalopathy in severe COVID-19: a cohort analysis of ICU patients. *Critical care (London, England)*. 2020;24(1):491. doi:10.1186/s13054-020-03200-1

38. Merad M, Blish CA, Sallusto F, Iwasaki A. The immunology and immunopathology of COVID-19. *Science*. 2022;375(6585):1122-1127. doi:10.1126/science.abm8108
39. Sposito B, Broggi A, Pandolfi L, et al. The interferon landscape along the respiratory tract impacts the severity of COVID-19. *Cell*. 2021;184(19):4953-4968.e16. doi:10.1016/j.cell.2021.08.016
40. André S, Picard M, Cezar R, et al. T cell apoptosis characterizes severe Covid-19 disease. *Cell Death and Differentiation*. 2022;29(8):1486-1499. doi:10.1038/s41418-022-00936-x
41. Lucas C, Wong P, Klein J, et al. Longitudinal analyses reveal immunological misfiring in severe COVID-19. *Nature*. 2020;584(7821):463-469. doi:10.1038/s41586-020-2588-y
42. Li S, Jiang L, Li X, et al. Clinical and pathological investigation of patients with severe COVID-19. *JCI Insight*. 2020;5(12). doi:10.1172/jci.insight.138070
43. Carsana L, Sonzogni A, Nasr A, et al. Pulmonary post-mortem findings in a series of COVID-19 cases from northern Italy: a two-centre descriptive study. *The Lancet. Infectious Diseases*. 2020;20(10):1135-1140. doi:10.1016/S1473-3099(20)30434-5
44. Edler C, Schröder AS, Aepfelbacher M, et al. Dying with SARS-CoV-2 infection-an autopsy study of the first consecutive 80 cases in Hamburg, Germany. *Int J Legal Med*. 2020;134(4):1275-1284. doi:10.1007/s00414-020-02317-w
45. Zhang Z, Zheng Y, Niu Z, et al. SARS-CoV-2 spike protein dictates syncytium-mediated lymphocyte elimination. *Cell Death and Differentiation*. 2021;28(9):2765-2777. doi:10.1038/s41418-021-00782-3
46. Musso N, Falzone L, Stracquadanio S, et al. Post-Mortem Detection of SARS-CoV-2 RNA in Long-Buried Lung Samples. *Diagnostics*. 2021;11(7):1158. doi:10.3390/diagnostics11071158
47. Hönzke K, Obermayer B, Mache C, et al. Human lungs show limited permissiveness for SARS-CoV-2 due to scarce ACE2 levels but virus-induced expansion of inflammatory macrophages. *Eur Respir J*. 2022;60(6). doi:10.1183/13993003.02725-2021

48. Wendisch D, Dietrich O, Mari T, et al. SARS-CoV-2 infection triggers profibrotic macrophage responses and lung fibrosis. *Cell*. 2021;184(26):6243-6261.e27. doi:10.1016/j.cell.2021.11.033
49. AWMF Leitlinienregister. Published May 22, 2023. Accessed June 4, 2023. https://register.awmf.org/de/leitlinien/detail/113-001LG
50. RKI - COVRIIN. Published June 4, 2023. Accessed June 4, 2023. https://www.rki.de/DE/Content/Kommissionen/COVRIIN/Therapie_Versorgung/FG_COVRIIN_Therapie_Versorgung_node.html
51. Therapeutics and COVID-19. Published June 2, 2023. Accessed June 4, 2023. https://www.who.int/teams/health-care-readiness/covid-19/therapeutics
52. Horby P, Lim WS, Emberson JR, et al. Dexamethasone in Hospitalized Patients with Covid-19. *N Engl J Med*. 2021;384(8):693-704. doi:10.1056/NEJMoa2021436
53. Kakarla R, Hur J, Kim YJ, Kim J, Chwae Y-J. Apoptotic cell-derived exosomes: messages from dying cells. *Exp Mol Med*. 2020;52(1):1-6. doi:10.1038/s12276-019-0362-8
54. Riedl SJ, Shi Y. Molecular mechanisms of caspase regulation during apoptosis. *Nat Rev Mol Cell Biol*. 2004;5(11):897-907. doi:10.1038/nrm1496
55. Patel V, Balakrishnan K, Keating MJ, Wierda WG, Gandhi V. Expression of executioner procaspases and their activation by a procaspase-activating compound in chronic lymphocytic leukemia cells. *Blood*. 2015;125(7):1126-1136. doi:10.1182/blood-2014-01-546796
56. Kerr JF, Wyllie AH, Currie AR. Apoptosis: a basic biological phenomenon with wide-ranging implications in tissue kinetics. *Br J Cancer*. 1972;26(4):239-257. doi:10.1038/bjc.1972.33
57. Horvitz HR. Genetic control of programmed cell death in the nematode Caenorhabditis elegans. *Cancer Res*. 1999;59(7 Suppl):1701s-1706s.
58. Elmore S. Apoptosis: a review of programmed cell death. *Toxicol Pathol*. 2007;35(4):495-516. doi:10.1080/01926230701320337
59. Savill J, Fadok V. Corpse clearance defines the meaning of cell death. *Nature*. 2000;407(6805):784-788. doi:10.1038/35037722

60. Wickman G, Julian L, Olson MF. How apoptotic cells aid in the removal of their own cold dead bodies. *Cell Death and Differentiation*. 2012;19(5):735-742. doi:10.1038/cdd.2012.25
61. Mariathasan S, Newton K, Monack DM, et al. Differential activation of the inflammasome by caspase-1 adaptors ASC and Ipaf. *Nature*. 2004;430(6996):213-218. doi:10.1038/nature02664
62. Bertheloot D, Latz E, Franklin BS. Necroptosis, pyroptosis and apoptosis: an intricate game of cell death. *Cell Mol Immunol*. 2021;18(5):1106-1121. doi:10.1038/s41423-020-00630-3
63. Vincent O'Brien. Viruses and apoptosis. *Journal of General Virology*. 1998;79(8):1833-1845. doi:10.1099/0022-1317-79-8-1833
64. Atkin-Smith GK, Duan M, Zanker DJ, et al. Monocyte apoptotic bodies are vehicles for influenza A virus propagation. *Commun Biol*. 2020;3(1):223. doi:10.1038/s42003-020-0955-8
65. Thomson BJ. Viruses and apoptosis. *International Journal of Experimental Pathology*. 2001;82(2):65-76. doi:10.1111/j.1365-2613.2001.iep0082-0065-x
66. Richard A, Tulasne D. Caspase cleavage of viral proteins, another way for viruses to make the best of apoptosis. *Cell Death Dis*. 2012;3(3):e277. doi:10.1038/cddis.2012.18
67. Hin Chu, Huiping Shuai, Yuxin Hou, et al. Targeting highly pathogenic coronavirus-induced apoptosis reduces viral pathogenesis and disease severity. *Sci Adv*. 2021;7(25). doi:10.1126/sciadv.abf8577
68. Sefik E, Qu R, Junqueira C, et al. Inflammasome activation in infected macrophages drives COVID-19 pathology. *Nature*. 2022;606(7914):585-593. doi:10.1038/s41586-022-04802-1
69. Pockros PJ, Schiff ER, Shiffman ML, et al. Oral IDN-6556, an antiapoptotic caspase inhibitor, may lower aminotransferase activity in patients with chronic hepatitis C. *Hepatology*. 2007;46(2):324-329. doi:10.1002/hep.21664
70. Matthay MA, Zemans RL. The acute respiratory distress syndrome: pathogenesis and treatment. *Annu Rev Pathol*. 2011;6:147-163. doi:10.1146/annurev-pathol-011110-130158

71. Barreyro FJ, Holod S, Finocchietto PV, et al. The pan-caspase inhibitor Emricasan (IDN-6556) decreases liver injury and fibrosis in a murine model of non-alcoholic steatohepatitis. *Liver International*. 2015;35(3):953-966. doi:10.1111/liv.12570
72. Hoglen NC, Chen L-S, Fisher CD, Hirakawa BP, Groessl T, Contreras PC. Characterization of IDN-6556 (3-2-(2-tert-butyl-phenylaminooxalyl)-amino-propionylamino-4-oxo-5-(2,3,5,6-tetrafluoro-phenoxy)-pentanoic acid): a liver-targeted caspase inhibitor. *J Pharmacol Exp Ther*. 2004;309(2):634-640. doi:10.1124/jpet.103.062034
73. Lekakis V, Cholongitas E. The impact of emricasan on chronic liver diseases: current data. *Clin J Gastroenterol*. 2022;15(2):271-285. doi:10.1007/s12328-021-01585-2
74. Conatus Pharmaceuticals Inc. A Placebo-Controlled, Multicenter, Double-Blind, Randomized, Pharmacokinetic and Pharmacodynamic Trial of IDN-6556 in Subjects With Acute-on-Chronic Liver Failure: NCT01937130, IDN-6556-02. Published April 11, 2016. Accessed June 5, 2023. https://clinicaltrials.gov/ct2/show/NCT01937130
75. Mehta G, Rousell S, Burgess G, et al. A Placebo-Controlled, Multicenter, Double-Blind, Phase 2 Randomized Trial of the Pan-Caspase Inhibitor Emricasan in Patients with Acutely Decompensated Cirrhosis. *J Clin Exp Hepatol*. 2018;8(3):224-234. doi:10.1016/j.jceh.2017.11.006
76. Weinberg EM, Curry MP, Frenette CT, et al. Multicenter, Double-Blind, Randomized Trial of Emricasan in Hepatitis C–Treated Liver Transplant Recipients With Residual Fibrosis or Cirrhosis. *Liver Transpl*. 2021;27(4):568-579. doi:10.1002/lt.25934
77. Elbekai RH, Paranjpe MG, Contreras PC, Spada A. Carcinogenicity assessment of the pan-caspase inhibitor, emricasan, in Tg.rasH2 mice. *Regul Toxicol Pharmacol*. 2015;72(2):169-178. doi:10.1016/j.yrtph.2015.04.007
78. Roumane A, Berthenet K, El Fassi C, Ichim G. Caspase-independent cell death does not elicit a proliferative response in melanoma cancer cells. *BMC Cell Biol*. 2018;19(1):11. doi:10.1186/s12860-018-0164-1

79. Xu M, Lee EM, Wen Z, et al. Identification of small-molecule inhibitors of Zika virus infection and induced neural cell death via a drug repurposing screen. *Nat Med*. 2016;22(10):1101-1107. doi:10.1038/nm.4184
80. Plassmeyer M, Alpan O, Corley MJ, et al. Caspases and therapeutic potential of caspase inhibitors in moderate-severe SARS-CoV-2 infection and long COVID. *Allergy*. 2022;77(1):118-129. doi:10.1111/all.14907
81. Histogen. Safety and Tolerability of Emricasan in Symptomatic Outpatients Diagnosed With Mild-COVID-19: NCT04803227, EMR-COV-PR001. Published January 4, 2022. Accessed June 9, 2023. https://clinicaltrials.gov/ct2/show/NCT04803227
82. Toptan T, Eckermann L, Pfeiffer AE, et al. Evaluation of a SARS-CoV-2 rapid antigen test: Potential to help reduce community spread? *Journal of Clinical Virology*. 2021;135:104713. doi:10.1016/j.jcv.2020.104713
83. Kohmer N, Toptan T, Pallas C, et al. The Comparative Clinical Performance of Four SARS-CoV-2 Rapid Antigen Tests and Their Correlation to Infectivity In Vitro. *Journal of Clinical Medicine*. 2021;10(2):328. doi:10.3390/jcm10020328
84. Plenzig S, Bojkova D, Held H, et al. Infectivity of deceased COVID-19 patients. *Int J Legal Med*. 2021;135(5):2055-2060. doi:10.1007/s00414-021-02546-7
85. Bojkova D, Reus P, Panosch L, et al. *Identification of Novel Antiviral Drug Candidates Using an Optimized SARS-CoV-2 Phenotypic Screening Platform*. 2022.
86. Bojkova D, Klann K, Koch B, et al. Proteomics of SARS-CoV-2-infected host cells reveals therapy targets. *Nature*. 2020;583(7816):469-472. doi:10.1038/s41586-020-2332-7
87. Kohmer N, Rabenau HF, Hoehl S, Kortenbusch M, Ciesek S, Berger A. Comparative analysis of point-of-care, high-throughput and laboratory-developed SARS-CoV-2 nucleic acid amplification tests (NATs). *J Virol Methods*. 2021;291:114102. doi:10.1016/j.jviromet.2021.114102
88. Cinatl J, Morgenstern B, Bauer G, Chandra P, Rabenau H, Doerr HW. Glycyrrhizin, an active component of liquorice roots, and replication of SARS-

associated coronavirus. *The Lancet*. 2003;361(9374):2045-2046. doi:10.1016/S0140-6736(03)13615-X

89. Cinatl J, Michaelis M, Morgenstern B, Doerr H. High-dose hydrocortisone reduces expression of the pro-inflammatory chemokines CXCL8 and CXCL10 in SARS coronavirus-infected intestinal cells. *Int J Mol Med*. 2005. doi:10.3892/ijmm.15.2.323
90. Toptan T, Hoehl S, Westhaus S, et al. Optimized qRT-PCR Approach for the Detection of Intra- and Extra-Cellular SARS-CoV-2 RNAs. *Int J Mol Sci*. 2020;21(12). doi:10.3390/ijms21124396
91. Hoehl S, Rabenau H, Berger A, et al. Evidence of SARS-CoV-2 Infection in Returning Travelers from Wuhan, China. *N Engl J Med*. 2020;382(13):1278-1280. doi:10.1056/NEJMc2001899
92. Tsang NNY, So HC, Ng KY, Cowling BJ, Leung GM, Ip DKM. Diagnostic performance of different sampling approaches for SARS-CoV-2 RT-PCR testing: a systematic review and meta-analysis. *The Lancet. Infectious Diseases*. 2021;21(9):1233-1245. doi:10.1016/S1473-3099(21)00146-8
93. Hou YJ, Chiba S, Halfmann P, et al. SARS-CoV-2 D614G variant exhibits efficient replication ex vivo and transmission in vivo. *Science*. 2020. doi:10.1126/science.abe8499
94. Sun L, Wang H, Wang Z, et al. Mixed lineage kinase domain-like protein mediates necrosis signaling downstream of RIP3 kinase. *Cell*. 2012;148(1-2):213-227. doi:10.1016/j.cell.2011.11.031
95. Modes of transmission of virus causing COVID-19: implications for IPC precaution recommendations. Published February 6, 2023. Accessed February 6, 2023. https://www.who.int/news-room/commentaries/detail/modes-of-transmission-of-virus-causing-covid-19-implications-for-ipc-precaution-recommendations
96. Li Q, Guan X, Wu P, et al. Early Transmission Dynamics in Wuhan, China, of Novel Coronavirus-Infected Pneumonia. *N Engl J Med*. 2020;382(13):1199-1207. doi:10.1056/NEJMoa2001316

97. Liu J, Liao X, Qian S, et al. Community Transmission of Severe Acute Respiratory Syndrome Coronavirus 2, Shenzhen, China, 2020. *Emerging Infectious Diseases*. 2020;26(6):1320-1323. doi:10.3201/eid2606.200239
98. van Kampen JJ, van de Vijver DA, Fraaij PL, et al. Shedding of infectious virus in hospitalized patients with coronavirus disease-2019 (COVID-19): duration and key determinants. *medRxiv*. 2020:2020.06.08.20125310. doi:10.1101/2020.06.08.20125310
99. Sonnleitner ST, Dorighi J, Jansen B, et al. Correction to: An in vitro model for assessment of SARS-CoV-2 infectivity by defining the correlation between virus isolation and quantitative PCR value: isolation success of SARS-CoV-2 from oropharyngeal swabs correlates negatively with Cq value. *Virology Journal*. 2021;18(1):82. doi:10.1186/s12985-021-01558-4
100. Bullard J, Dust K, Funk D, et al. Predicting Infectious Severe Acute Respiratory Syndrome Coronavirus 2 From Diagnostic Samples. *Clinical infectious diseases : an official publication of the Infectious Diseases Society of America*. 2020;71(10):2663-2666. doi:10.1093/cid/ciaa638
101. Yamada S, Fukushi S, Kinoshita H, et al. Assessment of SARS-CoV-2 infectivity of upper respiratory specimens from COVID-19 patients by virus isolation using VeroE6/TMPRSS2 cells. *BMJ Open Respiratory Research*. 2021;8(1):e000830. doi:10.1136/bmjresp-2020-000830
102. Singanayagam A, Patel M, Charlett A, et al. Duration of infectiousness and correlation with RT-PCR cycle threshold values in cases of COVID-19, England, January to May 2020. *Eurosurveillance*. 2020;25(32):2001483. doi:10.2807/1560-7917.ES.2020.25.32.2001483
103. Gallichotte EN, Quicke KM, Sexton NR, et al. Early Adoption of Longitudinal Surveillance for SARS-CoV-2 among Staff in Long-Term Care Facilities: Prevalence, Virologic and Sequence Analysis. *Microbiology Spectrum*. 2021;9(3):e0100321. doi:10.1128/Spectrum.01003-21
104. RKI - Coronavirus SARS-CoV-2 - Hinweise zur Testung von Patientinnen und Patienten auf SARS-CoV-2. Published March 18, 2023. Accessed March 22, 2023.

https://www.rki.de/DE/Content/InfAZ/N/Neuartiges_Coronavirus/Vorl_Testung_nCoV.html

105. Tallmadge RL, Laverack M, Cronk B, et al. Viral RNA Load and Infectivity of SARS-CoV-2 in Paired Respiratory and Oral Specimens from Symptomatic, Asymptomatic, or Postsymptomatic Individuals. *Microbiology Spectrum*. 2022;10(3):e0226421. doi:10.1128/spectrum.02264-21

106. Clinical and virologic characteristics of the first 12 patients with coronavirus disease 2019 (COVID-19) in the United States. *Nat Med*. 2020;26(6):861-868. doi:10.1038/s41591-020-0877-5

107. La Scola B, Le Bideau M, Andreani J, et al. Viral RNA load as determined by cell culture as a management tool for discharge of SARS-CoV-2 patients from infectious disease wards. *Eur J Clin Microbiol Infect Dis*. 2020;39(6):1059-1061. doi:10.1007/s10096-020-03913-9

108. Wang W, Xu Y, Gao R, et al. Detection of SARS-CoV-2 in Different Types of Clinical Specimens. *JAMA*. 2020;323(18):1843-1844. doi:10.1001/jama.2020.3786

109. Preparedness E. Diagnostic testing for SARS-CoV-2. *World Health Organization.* Published September 11, 2020. Accessed March 23, 2023. https://www.who.int/publications/i/item/diagnostic-testing-for-sars-cov-2.

110. World Health Organization. *Laboratory Testing for Coronavirus Disease (COVID-19) in Suspected Human Cases: Interim Guidance, 19 March 2020*; 2020; WHO/COVID-19/laboratory/2020.5. https://apps.who.int/iris/handle/10665/331501.

111. Who Headquarters. Laboratory testing of 2019 novel coronavirus (2019-nCoV) in suspected human cases: interim guidance, 17 January 2020. *World Health Organization.* Published January 17, 2020. Accessed March 23, 2023. https://www.who.int/publications/i/item/laboratory-testing-of-2019-novel-coronavirus-(-2019-ncov)-in-suspected-human-cases-interim-guidance-17-january-2020.

112. Hammitt LL, Kazungu S, Welch S, et al. Added value of an oropharyngeal swab in detection of viruses in children hospitalized with lower respiratory tract

infection. *Journal of clinical microbiology*. 2011;49(6):2318-2320. doi:10.1128/JCM.02605-10

113. Huang C-G, Lee K-M, Hsiao M-J, et al. Culture-Based Virus Isolation To Evaluate Potential Infectivity of Clinical Specimens Tested for COVID-19. *Journal of clinical microbiology*. 2020;58(8). doi:10.1128/JCM.01068-20

114. Uwamino Y, Nagata M, Aoki W, et al. Accuracy of rapid antigen detection test for nasopharyngeal swab specimens and saliva samples in comparison with RT-PCR and viral culture for SARS-CoV-2 detection. *J Infect Chemother*. 2021;27(7):1058-1062. doi:10.1016/j.jiac.2021.04.010

115. Ren L-L, Wang Y-M, Wu Z-Q, et al. Identification of a novel coronavirus causing severe pneumonia in human: a descriptive study. *Chinese Medical Journal*. 2020;133(9):1015-1024. doi:10.1097/CM9.0000000000000722

116. Patrucco F, Albera C, Bellocchia M, et al. SARS-CoV-2 Detection on Bronchoalveolar Lavage: An Italian Multicenter experience. *Respiration*. 2020;99(11):970-978. doi:10.1159/000511964

117. Casagrande M, Fitzek A, Spitzer MS, et al. Presence of SARS-CoV-2 RNA in the Cornea of Viremic Patients With COVID-19. *JAMA Ophthalmol*. 2021;139(4):383-388. doi:10.1001/jamaophthalmol.2020.6339

118. Bogdanović M, Skadrić I, Atanasijević T, et al. Case Report: Post-mortem Histopathological and Molecular Analyses of the Very First Documented COVID-19-Related Death in Europe. *Front Med*. 2021;8:612758. doi:10.3389/fmed.2021.612758

119. Plenzig S, Holz F, Bojkova D, et al. Detection and infectivity of SARS-CoV-2 in exhumated corpses. *Int J Legal Med*. 2021;135(6):2531-2536. doi:10.1007/s00414-021-02670-4

120. Stein SR, Ramelli SC, Grazioli A, et al. SARS-CoV-2 infection and persistence in the human body and brain at autopsy. *Nature*. 2022;612(7941):758-763. doi:10.1038/s41586-022-05542-y

121. Zacharias M, Stangl V, Thüringer A, et al. Rapid Antigen Test for Postmortem Evaluation of SARS-CoV-2 Carriage. *Emerging Infectious Diseases*. 2021;27(6):1734-1737. doi:10.3201/eid2706.210226

122. Saitoh H, Sakai-Tagawa Y, Nagasawa S, et al. High titers of infectious SARS-CoV-2 in corpses of patients with COVID-19. *Int J Infect Dis*. 2023;129:103-109. doi:10.1016/j.ijid.2023.01.046

123. Sriwijitalai W, Wiwanitkit V. COVID-19 in forensic medicine unit personnel: Observation from Thailand. *Journal of Forensic and Legal Medicine*. 2020;72:101964. doi:10.1016/j.jflm.2020.101964

124. Schröder AS, Edler C, Ondruschka B, et al. The handling of SARS-CoV-2 associated deaths - infectivity of the body. *Forensic Sci Med Pathol*. 2021;17(3):411-418. doi:10.1007/s12024-021-00379-9

125. Tavazzi G, Pellegrini C, Maurelli M, et al. Myocardial localization of coronavirus in COVID-19 cardiogenic shock. *European Journal of Heart Failure*. 2020;22(5):911-915. doi:10.1002/ejhf.1828

126. Putra SP, Hidayat T, Zhuhra RT. SARS-CoV-2 persistence and infectivity in COVID-19 corpses: a systematic review. *Forensic Science, Medicine, and Pathology*. 2023;19(1):94-102. doi:10.1007/s12024-022-00518-w

127. Puelles VG, Lütgehetmann M, Lindenmeyer MT, et al. Multiorgan and Renal Tropism of SARS-CoV-2. *N Engl J Med*. 2020;383(6):590-592. doi:10.1056/NEJMc2011400

128. Gupta A, Madhavan MV, Sehgal K, et al. Extrapulmonary manifestations of COVID-19. *Nat Med*. 2020;26(7):1017-1032. doi:10.1038/s41591-020-0968-3

129. Wanner N, Andrieux G, Badia-i-Mompel P, et al. Molecular consequences of SARS-CoV-2 liver tropism. *Nat Metab*. 2022;4(3):310-319. doi:10.1038/s42255-022-00552-6

130. Braun F, Lütgehetmann M, Pfefferle S, et al. SARS-CoV-2 renal tropism associates with acute kidney injury. *The Lancet*. 2020;396(10251):597-598. doi:10.1016/S0140-6736(20)31759-1

131. Bradley BT, Maioli H, Johnston R, et al. Histopathology and ultrastructural findings of fatal COVID-19 infections in Washington State: a case series. *Lancet (London, England)*. 2020;396(10247):320-332. doi:10.1016/S0140-6736(20)31305-2

132. Varga Z, Flammer AJ, Steiger P, et al. Endothelial cell infection and endotheliitis in COVID-19. *The Lancet*. 2020;395(10234):1417-1418. doi:10.1016/S0140-6736(20)30937-5

133. Bhatnagar J, Gary J, Reagan-Steiner S, et al. Evidence of Severe Acute Respiratory Syndrome Coronavirus 2 Replication and Tropism in the Lungs, Airways, and Vascular Endothelium of Patients With Fatal Coronavirus Disease 2019: An Autopsy Case Series. *J Infect Dis*. 2021;223(5):752-764. doi:10.1093/infdis/jiab039

134. Delorey TM, Ziegler CGK, Heimberg G, et al. COVID-19 tissue atlases reveal SARS-CoV-2 pathology and cellular targets. *Nature*. 2021;595(7865):107-113. doi:10.1038/s41586-021-03570-8

135. Lehmann M, Allers K, Heldt C, et al. Human small intestinal infection by SARS-CoV-2 is characterized by a mucosal infiltration with activated CD8+ T cells. *Mucosal Immunology*. 2021;14(6):1381-1392. doi:10.1038/s41385-021-00437-z

136. Chu H, Chan JF-W, Wang Y, et al. SARS-CoV-2 Induces a More Robust Innate Immune Response and Replicates Less Efficiently Than SARS-CoV in the Human Intestines: An Ex Vivo Study With Implications on Pathogenesis of COVID-19. *Cellular and Molecular Gastroenterology and Hepatology*. 2021;11(3):771-781. doi:10.1016/j.jcmgh.2020.09.017

137. Zhou C, Byard RW. Factors and processes causing accelerated decomposition in human cadavers - An overview. *Journal of Forensic and Legal Medicine*. 2011;18(1):6-9. doi:10.1016/j.jflm.2010.10.003

138. Wichmann D, Sperhake J-P, Lütgehetmann M, et al. Autopsy Findings and Venous Thromboembolism in Patients With COVID-19: A Prospective Cohort Study. *Annals of Internal Medicine*. 2020;173(4):268-277. doi:10.7326/M20-2003

139. Jeong HW, Kim S-M, Kim H-S, et al. Viable SARS-CoV-2 in various specimens from COVID-19 patients. *Clinical microbiology and infection : the official publication of the European Society of Clinical Microbiology and Infectious Diseases*. 2020;26(11):1520-1524. doi:10.1016/j.cmi.2020.07.020

140. van Doremalen N, Bushmaker T, Morris DH, et al. Aerosol and Surface Stability of SARS-CoV-2 as Compared with SARS-CoV-1. *N Engl J Med*. 2020;382(16):1564-1567. doi:10.1056/NEJMc2004973

141. Rabenau HF, Cinatl J, Morgenstern B, Bauer G, Preiser W, Doerr HW. Stability and inactivation of SARS coronavirus. *Med Microbiol Immunol*. 2005;194(1-2):1-6. doi:10.1007/s00430-004-0219-0

142. Turner JS, O'Halloran JA, Kalaidina E, et al. SARS-CoV-2 mRNA vaccines induce persistent human germinal centre responses. *Nature*. 2021;596(7870):109-113. doi:10.1038/s41586-021-03738-2

143. Sterlin D, Mathian A, Miyara M, et al. IgA dominates the early neutralizing antibody response to SARS-CoV-2. *Sci Transl Med*. 2021;13(577). doi:10.1126/scitranslmed.abd2223

144. Bojkova D, Bechtel M, McLaughlin K-M, et al. Aprotinin Inhibits SARS-CoV-2 Replication. *Cells*. 2020;9(11):2377. doi:10.3390/cells9112377

145. van Wetering S, van der Linden AC, van Sterkenburg MA, et al. Regulation of SLPI and elafin release from bronchial epithelial cells by neutrophil defensins. *American journal of physiology. Lung cellular and molecular physiology*. 2000;278(1):L51-8. doi:10.1152/ajplung.2000.278.1.L51

146. Liao Y, Li X, Mou T, et al. Distinct infection process of SARS-CoV-2 in human bronchial epithelial cell lines. *Journal of Medical Virology*. 2020;92(11):2830-2838. doi:10.1002/jmv.26200

147. Ogando NS, Dalebout TJ, Zevenhoven-Dobbe JC, et al. SARS-coronavirus-2 replication in Vero E6 cells: replication kinetics, rapid adaptation and cytopathology. *Journal of General Virology*. 2020;101(9):925-940. doi:10.1099/jgv.0.001453

148. Hoffmann M, Kleine-Weber H, Schroeder S, et al. SARS-CoV-2 Cell Entry Depends on ACE2 and TMPRSS2 and Is Blocked by a Clinically Proven Protease Inhibitor. *Cell*. 2020;181(2):271-280.e8. doi:10.1016/j.cell.2020.02.052

149. Koch J, Uckeley ZM, Doldan P, Stanifer M, Boulant S, Lozach P-Y. TMPRSS2 expression dictates the entry route used by SARS-CoV-2 to infect

host cells. *The EMBO Journal*. 2021;40(16):e107821. doi:10.15252/embj.2021107821

150. Lamers MM, Mykytyn AZ, Breugem TI, et al. Human airway cells prevent SARS-CoV-2 multibasic cleavage site cell culture adaptation. *eLife*. 2021;10. doi:10.7554/eLife.66815

151. Mykytyn AZ, Breugem TI, Riesebosch S, et al. SARS-CoV-2 entry into human airway organoids is serine protease-mediated and facilitated by the multibasic cleavage site. *eLife*. 2021;10. doi:10.7554/eLife.64508

152. Shirato K, Kawase M, Matsuyama S. Wild-type human coronaviruses prefer cell-surface TMPRSS2 to endosomal cathepsins for cell entry. *Virology*. 2018;517:9-15. doi:10.1016/j.virol.2017.11.012

153. Shirato K, Kanou K, Kawase M, Matsuyama S. Clinical Isolates of Human Coronavirus 229E Bypass the Endosome for Cell Entry. *J Virol*. 2017;91(1). doi:10.1128/JVI.01387-16

154. Cinatl J, Morgenstern B, Bauer G, Chandra P, Rabenau H, Doerr HW. Treatment of SARS with human interferons. *Lancet (London, England)*. 2003;362(9380):293-294. doi:10.1016/s0140-6736(03)13973-6

155. Ozono S, Zhang Y, Ode H, et al. SARS-CoV-2 D614G spike mutation increases entry efficiency with enhanced ACE2-binding affinity. *Nat Commun*. 2021;12(1):848. doi:10.1038/s41467-021-21118-2

156. Chu H, Chan JF-W, Yuen TT-T, et al. Comparative tropism, replication kinetics, and cell damage profiling of SARS-CoV-2 and SARS-CoV with implications for clinical manifestations, transmissibility, and laboratory studies of COVID-19: an observational study. *The Lancet Microbe*. 2020;1(1):e14-e23. doi:10.1016/S2666-5247(20)30004-5

157. Nextstrain / ncov / gisaid / global / 6m. Published March 23, 2023. Accessed March 28, 2023. https://nextstrain.org/ncov/gisaid/global/6m?c=S1_mutations&tl=pango_lineage

158. Rajah MM, Hubert M, Bishop E, et al. SARS-CoV-2 Alpha, Beta, and Delta variants display enhanced Spike-mediated syncytia formation. *The EMBO Journal*. 2021;40(24):e108944. doi:10.15252/embj.2021108944

159. Sanders DW, Jumper CC, Ackerman PJ, et al. SARS-CoV-2 requires cholesterol for viral entry and pathological syncytia formation. *eLife Sciences Publications, Ltd.* Published April 23, 2021. Accessed March 29, 2023. https://elifesciences.org/articles/65962.

160. Buchrieser J, Dufloo J, Hubert M, et al. Syncytia formation by SARS-CoV-2-infected cells. *The EMBO Journal*. 2020;39(23):e106267. doi:10.15252/embj.2020106267

161. Plante JA, Liu Y, Liu J, et al. Spike mutation D614G alters SARS-CoV-2 fitness. *Nature*. 2021;592(7852):116-121. doi:10.1038/s41586-020-2895-3

162. Plavec Z, Domanska A, Liu X, et al. SARS-CoV-2 Production, Purification Methods and UV Inactivation for Proteomics and Structural Studies. *Viruses*. 2022;14(9):1989. doi:10.3390/v14091989

163. Kordyukova LV, Moiseenko AV, Serebryakova MV, et al. Structural and Immunoreactivity Properties of the SARS-CoV-2 Spike Protein upon the Development of an Inactivated Vaccine. *Viruses*. 2023;15(2):480. doi:10.3390/v15020480

164. Ren Y, an Wang, Fang Y, et al. SARS-CoV-2 Membrane Glycoprotein M Triggers Apoptosis With the Assistance of Nucleocapsid Protein N in Cells. *Front Cell Infect Microbiol*. 2021;11:706252. doi:10.3389/fcimb.2021.706252

165. Tsoi H, Li L, Chen ZS, Lau K-F, Tsui SKW, Chan HYE. The SARS-coronavirus membrane protein induces apoptosis via interfering with PDK1-PKB/Akt signalling. *Biochem J*. 2014;464(3):439-447. doi:10.1042/BJ20131461

166. Ren Y, Shu T, Di Wu, et al. The ORF3a protein of SARS-CoV-2 induces apoptosis in cells. *Cell Mol Immunol*. 2020;17(8):881-883. doi:10.1038/s41423-020-0485-9

167. Pizzorno A, Padey B, Julien T, et al. Characterization and Treatment of SARS-CoV-2 in Nasal and Bronchial Human Airway Epithelia. *CR Med*. 2020;1(4):100059. doi:10.1016/j.xcrm.2020.100059

168. Chan JF-W, Zhang AJ, Yuan S, et al. Simulation of the Clinical and Pathological Manifestations of Coronavirus Disease 2019 (COVID-19) in a Golden Syrian Hamster Model: Implications for Disease Pathogenesis and

Transmissibility. *Clinical infectious diseases : an official publication of the Infectious Diseases Society of America*. 2020;71(9):2428-2446. doi:10.1093/cid/ciaa325

169. Liu Y, Garron TM, Chang Q, et al. Cell-Type Apoptosis in Lung during SARS-CoV-2 Infection. *Pathogens*. 2021;10(5). doi:10.3390/pathogens10050509

170. Rendeiro AF, Ravichandran H, Bram Y, et al. The spatial landscape of lung pathology during COVID-19 progression. *Nature*. 2021;593(7860):564-569. doi:10.1038/s41586-021-03475-6

171. Karki R, Sharma BR, Tuladhar S, et al. Synergism of TNF-α and IFN-γ Triggers Inflammatory Cell Death, Tissue Damage, and Mortality in SARS-CoV-2 Infection and Cytokine Shock Syndromes. *Cell*. 2021;184(1):149-168.e17. doi:10.1016/j.cell.2020.11.025

172. Majchrzak M, Poręba M. The roles of cellular protease interactions in viral infections and programmed cell death: a lesson learned from the SARS-CoV-2 outbreak and COVID-19 pandemic. *Pharmacol Rep*. 2022;74(6):1149-1165. doi:10.1007/s43440-022-00394-9

173. Tsuchiya K. Inflammasome-associated cell death: Pyroptosis, apoptosis, and physiological implications. *Microbiology and Immunology*. 2020;64(4):252-269. doi:10.1111/1348-0421.12771

174. Sun R, Jiang K, Zeng C, et al. Synergism of TNF-α and IFN-β triggers human airway epithelial cells death by apoptosis and pyroptosis. *Molecular Immunology*. 2023;153:160-169. doi:10.1016/j.molimm.2022.12.002

175. Baker JD, Uhrich RL, Kraemer GC, Love JE, Kraemer BC. A drug repurposing screen identifies hepatitis C antivirals as inhibitors of the SARS-CoV2 main protease. *PLOS ONE*. 2021;16(2):e0245962. doi:10.1371/journal.pone.0245962

176. Kim J, Zhang J, Cha Y, et al. Advanced bioinformatics rapidly identifies existing therapeutics for patients with coronavirus disease-2019 (COVID-19). *J Transl Med*. 2020;18(1):257. doi:10.1186/s12967-020-02430-9

177. Hammond J, Leister-Tebbe H, Gardner A, et al. Oral Nirmatrelvir for High-Risk, Nonhospitalized Adults with Covid-19. *N Engl J Med*. 2022;386(15):1397-1408. doi:10.1056/NEJMoa2118542

178. Jin Z, Du X, Xu Y, et al. Structure of Mpro from SARS-CoV-2 and discovery of its inhibitors. *Nature*. 2020;582(7811):289-293. doi:10.1038/s41586-020-2223-y

179. Shrestha A, Mehdizadeh Gohari I, McClane BA. RIP1, RIP3, and MLKL Contribute to Cell Death Caused by Clostridium perfringens Enterotoxin. *mBio*. 2019;10(6). doi:10.1128/mBio.02985-19

180. Li S, Zhang Y, Guan Z, et al. SARS-CoV-2 triggers inflammatory responses and cell death through caspase-8 activation. *Signal transduction and targeted therapy*. 2020;5(1):235. doi:10.1038/s41392-020-00334-0

181. Zhang D-W, Shao J, Lin J, et al. RIP3, an energy metabolism regulator that switches TNF-induced cell death from apoptosis to necrosis. *Science*. 2009;325(5938):332-336. doi:10.1126/science.1172308

182. Cho YS, Challa S, Moquin D, et al. Phosphorylation-driven assembly of the RIP1-RIP3 complex regulates programmed necrosis and virus-induced inflammation. *Cell*. 2009;137(6):1112-1123. doi:10.1016/j.cell.2009.05.037

183. Zhan C, Huang M, Yang X, Hou J. MLKL: Functions beyond serving as the Executioner of Necroptosis. *Theranostics*. 2021;11(10):4759-4769. doi:10.7150/thno.54072

184. Wang H, Sun L, Su L, et al. Mixed lineage kinase domain-like protein MLKL causes necrotic membrane disruption upon phosphorylation by RIP3. *Molecular cell*. 2014;54(1):133-146. doi:10.1016/j.molcel.2014.03.003

185. Upton JW, Kaiser WJ, Mocarski ES. Virus inhibition of RIP3-dependent necrosis. *Cell host & microbe*. 2010;7(4):302-313. doi:10.1016/j.chom.2010.03.006

186. Li X, Zhang Z, Wang Z, Gutiérrez-Castrellón P, Shi H. Cell deaths: Involvement in the pathogenesis and intervention therapy of COVID-19. *Sig Transduct Target Ther*. 2022;7(1):186. doi:10.1038/s41392-022-01043-6

187. Tang D, Kang R, Berghe TV, Vandenabeele P, Kroemer G. The molecular machinery of regulated cell death. *Cell Res*. 2019;29(5):347-364. doi:10.1038/s41422-019-0164-5

188. He S, Wang L, Miao L, et al. Receptor interacting protein kinase-3 determines cellular necrotic response to TNF-alpha. *Cell*. 2009;137(6):1100-1111. doi:10.1016/j.cell.2009.05.021

189. Jiao J, Wang Y, Ren P, Sun S, Wu M. Necrosulfonamide Ameliorates Neurological Impairment in Spinal Cord Injury by Improving Antioxidative Capacity. *Frontiers in pharmacology*. 2019;10:1538. doi:10.3389/fphar.2019.01538

190. Śliwka L, Wiktorska K, Suchocki P, et al. The Comparison of MTT and CVS Assays for the Assessment of Anticancer Agent Interactions. *PloS one*. 2016;11(5):e0155772. doi:10.1371/journal.pone.0155772

191. Rathkey JK, Zhao J, Liu Z, et al. Chemical disruption of the pyroptotic pore-forming protein gasdermin D inhibits inflammatory cell death and sepsis. *Science immunology*. 2018;3(26). doi:10.1126/sciimmunol.aat2738

Schriftliche Erklärung

Ich erkläre ehrenwörtlich, dass ich die dem Fachbereich Medizin der Johann Wolfgang Goethe-Universität Frankfurt am Main zur Promotionsprüfung eingereichte Dissertation mit dem Titel

Characterization of Antiviral Effects of Emricasan and SARS-CoV-2 Isolates in Vitro

in dem Institut für Medizinische Virologie der Goethe Universität Frankfurt am Main unter Betreuung und Anleitung von Prof. Dr. Denisa Bojkova mit Unterstützung durch Prof. Dr. Sandra Ciesek ohne sonstige Hilfe selbst durchgeführt und bei der Abfassung der Arbeit keine anderen als die in der Dissertation angeführten Hilfsmittel benutzt habe. Darüber hinaus versichere ich, nicht die Hilfe einer kommerziellen Promotionsvermittlung in Anspruch genommen zu haben.

Ich habe bisher an keiner in- oder ausländischen Universität ein Gesuch um Zulassung zur Promotion eingereicht*. Die vorliegende Arbeit wurde bisher nicht als Dissertation eingereicht.

Vorliegende Ergebnisse der Arbeit wurden (oder werden) in folgendem Publikationsorgan veröffentlicht:

Toptan T, Eckermann L, Pfeiffer AE, Hoehl S, Ciesek S, Drosten C, Corman VM. Evaluation of a SARS-CoV-2 rapid antigen test: Potential to help reduce community spread? J Clin Virol. 2021; Feb 135:104713. doi: 10.1016/.cv.2020.104713.

Kohmer N, Toptan T, Pallas C, Karaca O, Pfeiffer A, Westhaus S, Widera M, Berger A, Hoehl S, Kammel M, Ciesek S, Rabenau HF. The Comparative Clinical Performance of Four SARS-CoV-2 Rapid Antigen Tests and Their Correlation to Infectivity In Vitro.J Clin

Med. 2021;10(2):328. https://doi.org/10.3390/jcm10020328
Plenzig S, Bojkova D, Held H, Berger A, Holz F, Cinatl J, KettnerM, Pfeiffer A, Verhoff M A, Ciesek S. Infectivity of deceased COVID-19 patients. Int J Legal Med. 2021;135(5):2055-2060. doi:10.1007/s00414021-02546-7.

Bojkova D, Reus P, Panosch L, Bechtel M, Rothenburger T, Kandler JD, Pfeiffer A, Wagner JUG, Shumliakivska M, Dimmeler S, Olmer R, Martin U, Vondran FWR, Toptan T, Rothweiler F, Zehner R, Rabenau HF, Osman KL, Pullan ST, Carroll MW, Stack R, Ciesek S, Wass MN, Michaelis M, Cinatl J Jr. Identification of novel antiviral drug candidates using an optimized SARS-CoV-2 phenotypic screening platform. iScience. 2023 Feb 17;26(2):105944. doi: 10.1016/j.isci.2023.105944.

Berlin, 25.05.2023

(Ort, Datum) (Unterschrift)

*) im Falle des Nichtzutreffens entfernen